STUDY OF THE TIMING CHARACTERISTICS IN COAXIAL Ge(Li) DETECTORS

STUDY OF THE TIMING CHARASTERISTICS IN COAXIAL Ge(Li) DETECTORS

By

GEORGIA BINIKOU PANAGIOTOPOULOS, B.Sc.

A Thesis

Submitted to the Faculty of Graduate Studies
in Partial Fulfilment of the Requirements

for the Degree

Master of Science

McMaster University

July 1969

MASTER OF SCIENCE (1969) McMASTER UNIVERSITY
(Physics) Hamilton, Ontario.

TITLE: Study of the Timing Characteristics in Coaxial Ge(Li) Detectors

AUTHOR: Georgia Binikou Panagiotopoulos, B.Sc. (Athens University)

SUPERVISOR: Dr. T. J. Kennett

NUMBER OF PAGES: vi, 62

SCOPE AND CONTENTS:

This thesis deals with the theory and application of semi-conductor detectors to timing measurements. The theory section discusses the charge collection times in the coaxial detector. The third chapter describes the experimental procedure for the γ-γ coincidence work, and the fourth part reports the results of studies of the timing characteristics of the coaxial detector.

ACKNOWLEDGEMENTS

I wish to express appreciation to my Research Director, Dr. T. J. Kennett for his encouragement and guidance throughout this work.

I would also like to thank Dr. W. V. Prestwich for his assistance and advice. My thanks also to Mr. A. Colenbrander for his assistance with the computer programming.

TABLE OF CONTENTS

LIST OF ILLUSTRATIONS

CHAPTER I

INTRODUCTION

In the six years since lithium-drift germanium γ-ray spectrometers of high resolution were first described by Tavendale and Ewan[1] at the Chalk River Laboratories significant developments have taken place. Tavendale[2,3] has reported on the continued development of these devices. First the construction and performance of small, high resolution germanium detectors up to 2.0 cm^3 was reported. However the efficiency of these detectors was too low for many experiments, especially for γ-ray coincidence work. Therefore efforts have been made to increase efficiency by drifting deeper depletion layer diodes. Many single open-ended coaxially drifted diodes with sensitive volumes in the range of 16 to 54 cm^3 have been fabricated and studied[4,5]. These large volume germanium detectors have shown excellent performance as γ-ray spectrometers. The device was fabricated by first diffusing lithium into all surfaces of the crystal, excepting one-end, at the centre of which is located the p-contact. The lithium is then drifted into the crystal leaving a coaxial cone of p-type germanium at the centre. Surface treatments have been investigated by Armantrout[6] and also

by Fiedler[7].

Semiconductor particle detectors operate like ion chambers by collecting the charge liberated by an incident ionizing particle. However the potential distribution in a semiconductor is more complicated. Once inside the detector the particle produces a certain number of hole electron pairs corresponding to the energy that it loses in this region. This charge constitutes the signal information and its motion in the electric field across the device produces the current in the external circuit. Therefore when γ-rays interact with germanium detectors by the photo-electric effect, the Compton effect or by pair production, the resulting pulse is proportional to the energy and can be analyzed to obtain the spectral distribution.

Under certain circumstances, the charge carrier transit times in semiconductor detectors can be quite short. This presents the possibility of using such detectors in nanosecond-timing applications. Even though the transit times of the charge carriers across the depletion region may be short, the rise time at the amplifier input may be relatively long. Loss of charge in the Ge(Li) detectors can be attributed to the

prevention of charge carriers from traversing the entire voltage across the device. This can occur in two ways. Either carriers can be trapped in transit across the device or else they can recombine along the initial track.

Strauss, Larsen and Sifter (1966)[8] have reported a study of the distribution of pulse shapes from planar Ge(Li) detectors. Sakai and T. A. McMath[9] made measurements that cover planar and coaxial detectors. Timing studies have been carried out by H. L. Malm (1966)[10] and by Ewan et al[11].

This thesis reports the results of studies of the timing properties of coaxial diodes and the time resolution curves that can be obtained. We have used lithium-drifted germanium detectors in γ-γ coincidence studies where the experiment has been carried out using a plastic detector and a Ge(Li) detector as a coincidence spectrometer. There are limitations in the coincidence resolving times due to large variations in charge collection times which result from the non-uniformity of the electric field in the Ge(Li) detector. The pulse shapes from the Ge(Li) detector are not constant and the spread in time is appreciable. Thus in order to minimize the time spread leading edge timing was used and discrimination as low as possible. Leading edge timing was used because it yields better time resolution than the cross over pick off method. But even with leading edge timing some pulses will

trigger the discriminator later than the majority giving rise to a "tail" or assymetry to the time distribution.

CHAPTER II

THEORETICAL CALCULATIONS TIMING MEASUREMENTS IN Ge(Li) COUNTERS

2.1 Introduction

Semiconductor detectors depend on the production of free charge carriers in crystals by the interaction of incident particles with bound electrons. Solid state detectors are analogous to the well known gaseous ionization chamber. In an ionization chamber the incident particle produces electron-ion pairs; in a solid the incident particle produces electron-hole pairs.

Detection of the incident particle is then a problem of collection of the liberated charge by application of an electric field. Detection of γ-rays represents an almost ideal situation for a semiconductor detector from the point of view of charge collection. The interaction of a γ-ray in the detector produces a large number of electron-hole pairs which drift to the positive and negative electrodes respectively.

2.2 Outline of the Calculations

We consider a total charge Q_T created at a point $\vec{r}_o$, in the electric field environment $\vec{E}(\vec{r}_o)$. The velocity induced, in the low-field linear approximation, is given by

$$\vec{V}(\vec{r}_1) = \mu\vec{E}(\vec{r}_1)$$

where μ is the mobility approprite to the carrier type. From symmetry considerations, the position can be described by one co-ordinate, giving

$$V = \frac{dr}{dt} = \mu E(r), \; r = r_o \text{ for } t = 0.$$

The equation of motion can be solved using the integral

$$\int_{r_o}^{r} \frac{dr}{\mu E(r)} = t \quad \text{to give } r = r(t).$$

Thus we can write explicitly the time dependence

$$V(t) = \mu E(r(t)] \; .$$

The current induced by the motion of the carriers is given by

$$I = NS\dot{} \, ev$$

where N is the carrier density, and S the boundary surface area. The boundary is described by $r = r_1$.

The charge collected after a time t is given by

$$Q(t) = \int_o^t (N\mu eS)E[r(t)]dt \; .$$

Letting $r(t_{max}) = r_1$, then

$$Q_T = \int_o^{t_{max}} (N\mu eS)E[r(t)]dt$$

The fraction of charge collected after time t is thus

$$F(t) = \frac{Q(t)}{Q_T} = \frac{\int_o^t E\,[r(t)]dt}{\int_o^{t_{max}} E[r(t)]dt}$$

Therefore $Q(t) = K \int_o^t E[r(t)]dt$ where K accounts for the necessary units.

2.3 Cylindrical Counter

For a coaxial detector it is assumed that the inner and outer cylinders have radii r_1 and r_2 respectively (Figure (1)). For such a configuration the field is given by

$$E(r) = \frac{V_o}{r \ln(\frac{r_2}{r_1})} . \qquad (1)$$

When a γ-ray interacts with the detector, creating electron-hole pairs at a "point" at radius r_o, the motion of the electrons is described by the equation

$$\frac{dr}{dt} = \mu_e E(r) = \frac{\mu_e V_o}{r \ln(\frac{r_2}{r_1})} ,$$

the motion of the holes is described by the equation

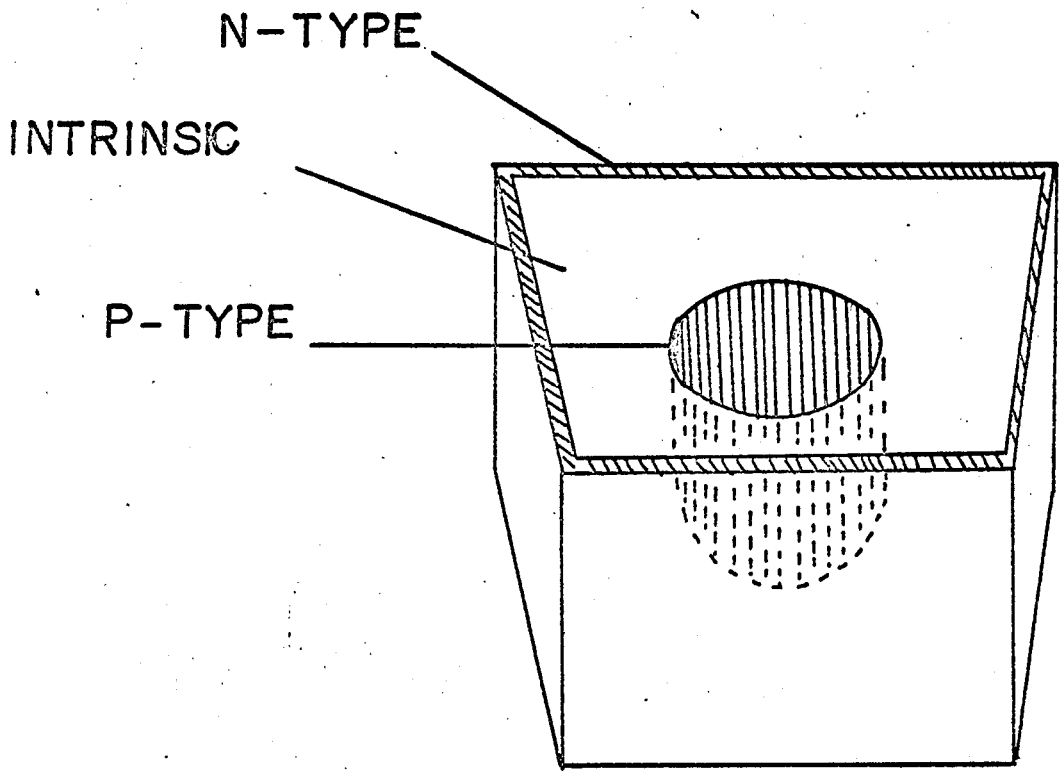

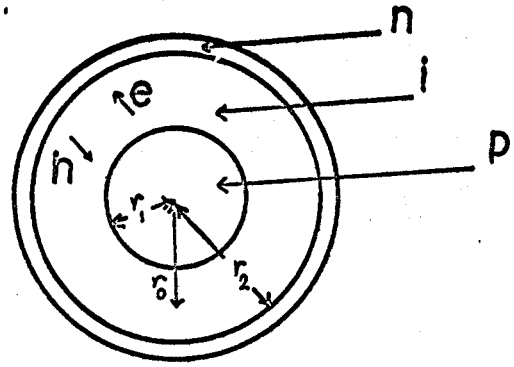

Fig. 1

Coaxial detector

$$\frac{dr}{dt} = \mu_h E(r) = \frac{\mu_h V_o}{r \ell n (\frac{r_2}{r_1})} ,$$

where μ_e is the electron mobility and μ_h is the hole mobility. In our case it is assumed to be the same for electrons and holes i.e. $-\mu_e = \mu_h = \mu = 4\times10^3$ cm^2/volt.sec. When charges are in motion current flows which when integrated upon stray capacitance yields a voltage. Employing the equation of motion for the electron

$$\frac{dr}{dt} = \frac{\mu_e V_o}{r \ell n (\frac{r_2}{r_1})} .$$

equation (2) can be calculated, i.e.

$$\int_o^t \frac{\mu V_o}{\ell n (\frac{r_2}{r_1})} = \int_{r_o}^{r} r \, dr \qquad (2)$$

where r_o is the formation point and t is the time required for the electrons to move to the position r . So for carriers moving towards the inner radius r_1 we will have

$$r = [r_o - \frac{2\mu V_o t}{\ell n (\frac{r_2}{r_1})}]^{\frac{1}{2}} \qquad (3)$$

Substituting equation (3) into equation (2) and integrating from the zero to time t the charge of holes is taken

$$Q_1 = \int_o^t idt = \int_o^t \frac{\mu V_o}{\ell n(\frac{r_2}{r_1})} \frac{dt}{[r_o^2 - \frac{2\mu V_o t}{\ell n(\frac{r_2}{r_1})}]^{\frac{1}{2}}}$$

or

$$Q_1 = r_o - [r_o^2 - \frac{2\mu V_o t}{\ell n(\frac{r_2}{r_1})}]^{\frac{1}{2}} \qquad (4)$$

when

$$r = r_1 \quad , \; t = t_{max}$$

hence from (3) we have

$$t_{max1} = \frac{\ell n(\frac{r_2}{r_1})}{2\mu V_o} (r_o^2 - r_1^2) \; . \qquad (5)$$

For carriers moving towards the outer radius r_2 we have

$$r = [r_o^2 + \frac{2\mu V_o t}{\ell n(\frac{r_2}{r_1})}]^{\frac{1}{2}} \qquad (6)$$

We substitute equation (6) into equation (2), hence the charge Q_2 induced by electrons is given by

$$Q_2 = \int_o^t idt = \int_o^t \frac{\mu V_o}{\ell n(\frac{r_2}{r_1})} \frac{dt}{[r_o^2 + \frac{2\mu V_o t}{\ell n(\frac{r_2}{r_1})}]^{\frac{1}{2}}}$$

$$Q_2 = [r_o^2 + \frac{2\mu V_o t}{\ell n(\frac{r_2}{r_1})}]^{\frac{1}{2}} - r_o \quad . \tag{7}$$

When $r = r_2$, $t = t_{max}$, hence from (6) we get

$$t_{max2} = \frac{\ell n(\frac{r_2}{r_1})}{2\mu V_o} (r_2^2 - r_o^2) \quad . \tag{8}$$

Using a transformation in which the r values are in mm and

$$\frac{\ell n(\frac{r_2}{r_1})}{2\mu V_o} = 1$$

the Q_1 and Q_2 are given by

$$\begin{aligned} Q_1 &= r_o - (r_o^2 - t)^{\frac{1}{2}} \\ Q_2 &= (r_o^2 + t)^{\frac{1}{2}} - r_o \end{aligned} \tag{9}$$

and the maximum times by

$$t_{max1} = r_o^2 - r_1^2 \quad , \quad t_{max2} = r_2^2 - r_o^2 \quad .$$

Therefore the charge induced by electrons and holes and the time limits in the two cases are given respectively by

$$Q_1 = r_o - (r_o^2 - t)^{\frac{1}{2}} \quad \text{where} \quad 0 \leq t \leq r_o^2 - r_1^2$$

$$Q_2 = (r_o^2 + t)^{\frac{1}{2}} - r_o \quad \text{where} \quad 0 \leq t \leq r_2^2 - r_o^2$$

A typical example of these functions is fig. (1) when ionization occurs at $r_o = \bar{r}_o = (\frac{r_1^2+r_2^2}{2})^{\frac{1}{2}}$ the times of collection are equal.

when $r_o < \bar{r}_o$ Q_1 ends first and

when $r_o > \bar{r}_o$ Q_2 ends first.

So we have to examine these two cases and find the total charge and the time limits in each case.

CASE (a) Q_1 ENDS FIRST

The total charge will be

$$Q = Q_1 + Q_2 = (r_o^2 + t)^{\frac{1}{2}} - (r_o^2 - t)^{\frac{1}{2}}, \quad 0 \leq t \leq r_o^2 - r_1^2 \quad (11)$$

But if we substitute the maximum time into the equation $Q_1 = r_o - (r_o^2 - t)^{\frac{1}{2}}$ we will get

$$Q_1 = r_o - r_1$$

hence (11) becomes

$$Q = (r_o^2 + t)^{\frac{1}{2}} - r_1 \quad , \quad r_o^2 - r_1^2 \leq t \leq r_2^2 - r_o^2$$

CASE (b) Q_2 ENDS FIRST

The total charge will be

$$Q_1 = Q_1 + Q_2 = (r_o^2 + t)^{\frac{1}{2}} - (r_o^2 - t)^{\frac{1}{2}} \quad , \quad 0 \leq t \leq r_2^2 - r_o^2 \, .$$

Substituting the time $t_{max2} = r_2^2 - r_o^2$ into $Q_2 = (r_o^2 + t)^{\frac{1}{2}} - r_o$ we have $Q_2 = r_2 - r_o$.

Therefore

$$Q = r_2 - (r_o^2 - t)^{\frac{1}{2}} \quad , \quad r_2^2 - r_o^2 \leq t \leq r_o^2 - r_1^2 \qquad (12)$$

Fig. (2) shows the pulse shapes in the cylindrical counter. We see that the shape of these pulses depends upon the location of interaction. The electrons and holes contribute to the pulse amplitude in proportion to the fractional distance they travel to reach their respective electrodes. Thus if the interaction takes place in the "center" $r_o = (\frac{r_1^2+r_2^2}{2})^{\frac{1}{2}}$ of the detector, the two carrier types would contribute equally to the resulting pulse, whereas if the interaction takes place near one of the electrodes the resulting pulse would correspond to the charge induced by only one type of carrier.

So in the case where the carriers have to travel only half the detector width the pulse would have a fast rise as depicted by wave form(7) in figure (2). If one type of carrier must cross the full width of the detector it would require twice as much time, as described by wave form(10). Most signals are likely to have collection times which are longer than (7) but shorter than (10). Their initial slope is the same as that of (7) but as the holes or electrons reach their collecting electrode the slope changes.

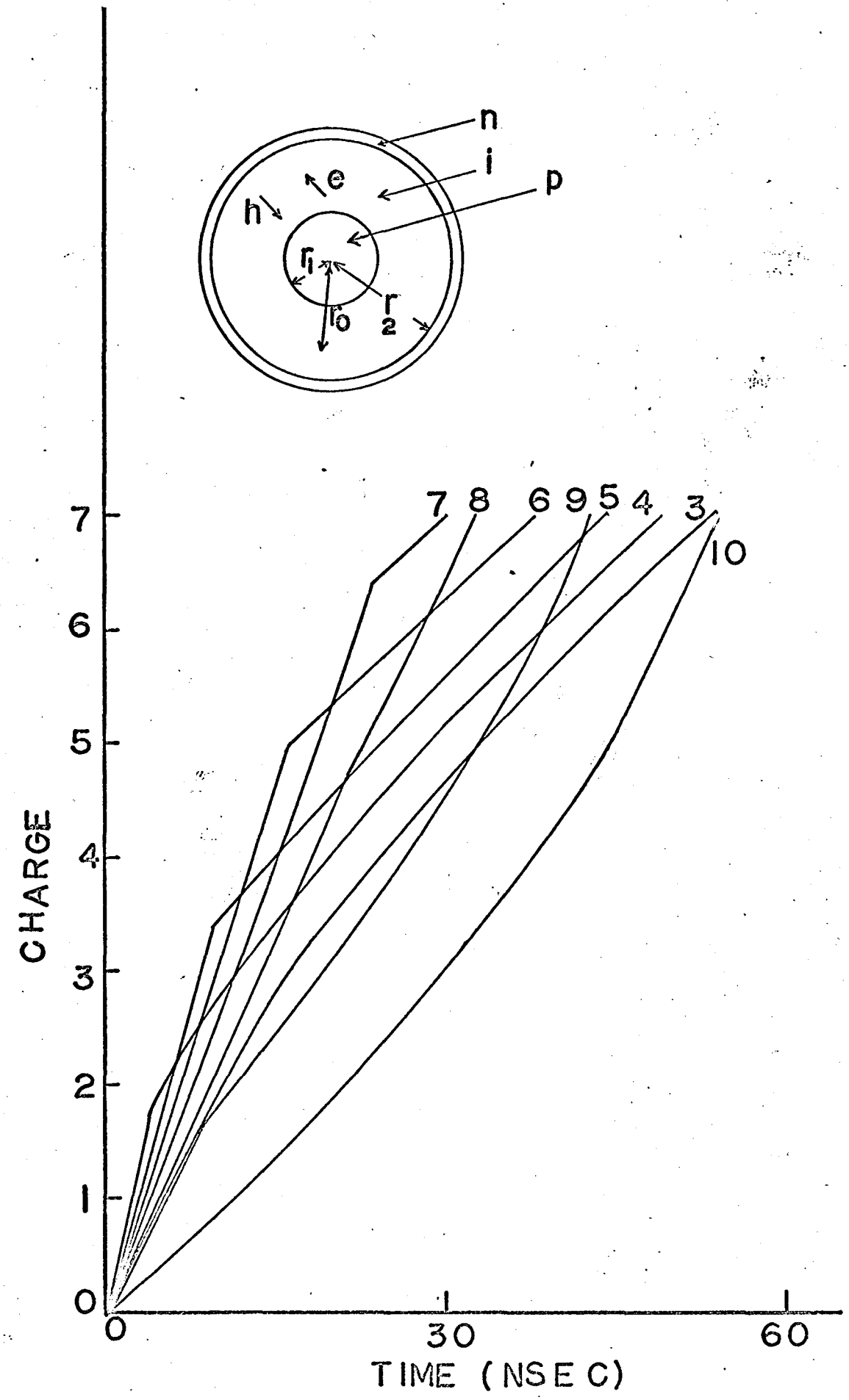

Fig. 2 Pulse shapes in a cylindrical counter

2.4 Spherical Counter

For a coaxial spherical detector it is assumed that the inner and outer hemispheres have radii r_1 and r_2 respectively (Figure (1)). For such a configuration the field is given by

$$E(r) = \frac{k}{r^2}$$

where k is a constant. The equation of motion is

$$\frac{dr}{dt} = \mu E(r) = \frac{\mu k}{r^2} \qquad (13)$$

where μ is the electron and hole mobility. If we integrate (13) we have:

$$\int_{r_o}^{r} r^2 dr = \int_{o}^{t} \mu k dt$$

$$\frac{r^3}{3}\Big]_{r_o}^{r} = \mu kt\Big]_{o}^{t} \quad , \quad \frac{r^3}{3} - \frac{r_o^3}{3} = \mu kt.$$

For carriers moving towards r_1 it will be

$$\frac{r^3}{3} - \frac{r_o^3}{3} = -\mu kt, \text{ because holes are}$$

moving towards r_1.

Therefore

$$r = (r_o^3 - 3\mu kt)^{1/3} \qquad (14)$$

or $$r^2 = (r_o^3 - 3\mu kt)^{2/3} .$$

So the charge induced by the holes is

$$Q_1 = \int_o^t i\,dt = \int_o^t \frac{\mu k}{r^2}\,dt = \int_o^t \frac{\mu k\,dt}{(r_o^3 - 3\mu k t)^{2/3}}$$

or

$$Q_1 = r_o - (r_o^3 - 3\mu k t)^{1/3} \tag{15}$$

when

$$r = r_1 \ , \ t = t_{max1}$$

hence from (14) we find the t_{max1} if we substitute

$$r = r_1 \qquad t_{max1} = \frac{r_o^3 - r_1^3}{3\mu k} \ .$$

Therefore

$$Q_1 = r_o - (r_o^3 - 3\mu k t)^{1/3} \text{ where } 0 \leq t \leq \frac{r_o^3 - r_1^3}{3\mu k}. \tag{16}$$

Similarly for carriers moving towards outer radius r_2 it will be

or

$$r = (r_o^3 + 3\mu k t)^{1/3}$$
$$r^2 = (r_o^3 + 3\mu k t)^{2/3} \ . \tag{17}$$

Therefore the charge induced by electrons is

$$Q_2 = \int_o^t \frac{\mu k}{r^2}\,dt = \int_o^t \frac{\mu k\,dt}{(r_o^3 + 3\mu k t)^{2/3}}$$

$$Q_2 = (r_o^3 + 3\mu k t)^{1/3} - r_o \tag{18}$$

when $r = r_2 \ , \ t = t_{max2}$

hence $$t_{max2} = \frac{r_2^3 - r_o^3}{3\mu k} \ .$$

Therefore

$$Q_2 = (r_o^3 + 3\mu kt)^{1/3} - r_o \text{ where } 0 \leq t \leq \frac{r_2^3 - r_o^3}{3\mu k} \quad (19)$$

Using a transformation in which the r values are in mm and $3\mu k = 1$ we have

$$Q_1 = r_o - (r_o^3 - t)^{1/3} \text{ where } 0 \leq t \leq r_o^3 - r_1^3$$
$$Q_2 = (r_o^3 + t)^{1/3} - r_o \text{ where } 0 \leq t \leq r_2^3 - r_o^3 . \quad (20)$$

Figure (2) is an example of these functions.

When ionization occurs at $r_o = \bar{r}_o = \left(\frac{r_1^3 + r_2^3}{2}\right)^{1/3}$ the times of collection are equal.

when $r_o < \bar{r}_o$ Q_1 ends first and

when $r_o > \bar{r}_o$ Q_2 ends first.

Examining the two cases we find the total charge and the time limits in each case.

CASE (a) Q_1 ENDS FIRST

The total charge is

$$Q = Q_1 + Q_2 = (r_o^3 + t)^{1/3} - (r_o^3 - t)^{1/3} , \ 0 \leq t \leq r_o^3 - r_1^3$$

But $Q_1 = r_o - r_1$ because of $t_{max1} = r_o^3 - r_1^3$

Therefore Q becomes

$$Q = (r_o^3 + t)^{1/3} - r_1, \ r_o^3 - r_1^3 \leq t \leq r_2^3 - r_o^3 \quad (21)$$

CASE (b) Q_2 ENDS FIRST

The total charge Q is

$$Q = Q_1 + Q_2 = (r_o^3 + t)^{1/3} - (r_o^3 - t)^{1/3},\ 0 \leq t \leq r_2^3 - r_o^3$$

But $Q_2 = r_2 - r_o$ because of $t_{max2} = r_2^3 - r_o^3$ therefore

$$Q = r_2 - (r_o^3 - t)^{1/3},\ r_2^3 = r_o^3 \leq t \leq r_o^3 - r_1^3 \qquad (22)$$

The results of these calculations can be seen in Figure (3) where the pulse shapes for the spherical counter have been plotted. It may be seen that the collection curves for the spherical case look like the ones for the cylindrical counter, but they are much slower. If the interaction takes place in the "center" $r_o = (\frac{r_1^2 + r_2^2}{2})^{1/3}$ of the detector, the two carrier types would contribute equally to the resulting pulse. If the interaction takes place near one of the electrodes the resulting pulse would correspond to the charge induced by only one type of carrier. Therefore when the carriers have to travel only about half the detector width the pulse would have a fast rise as depicted by waveform (8). if one type of carrier must cross the full width of the detector it would require almost twice as much time as described by waveform (10). So the most signals have collection times which are longer than (8) and shorter than (10).

Thus the similarity of the pulse shapes of the

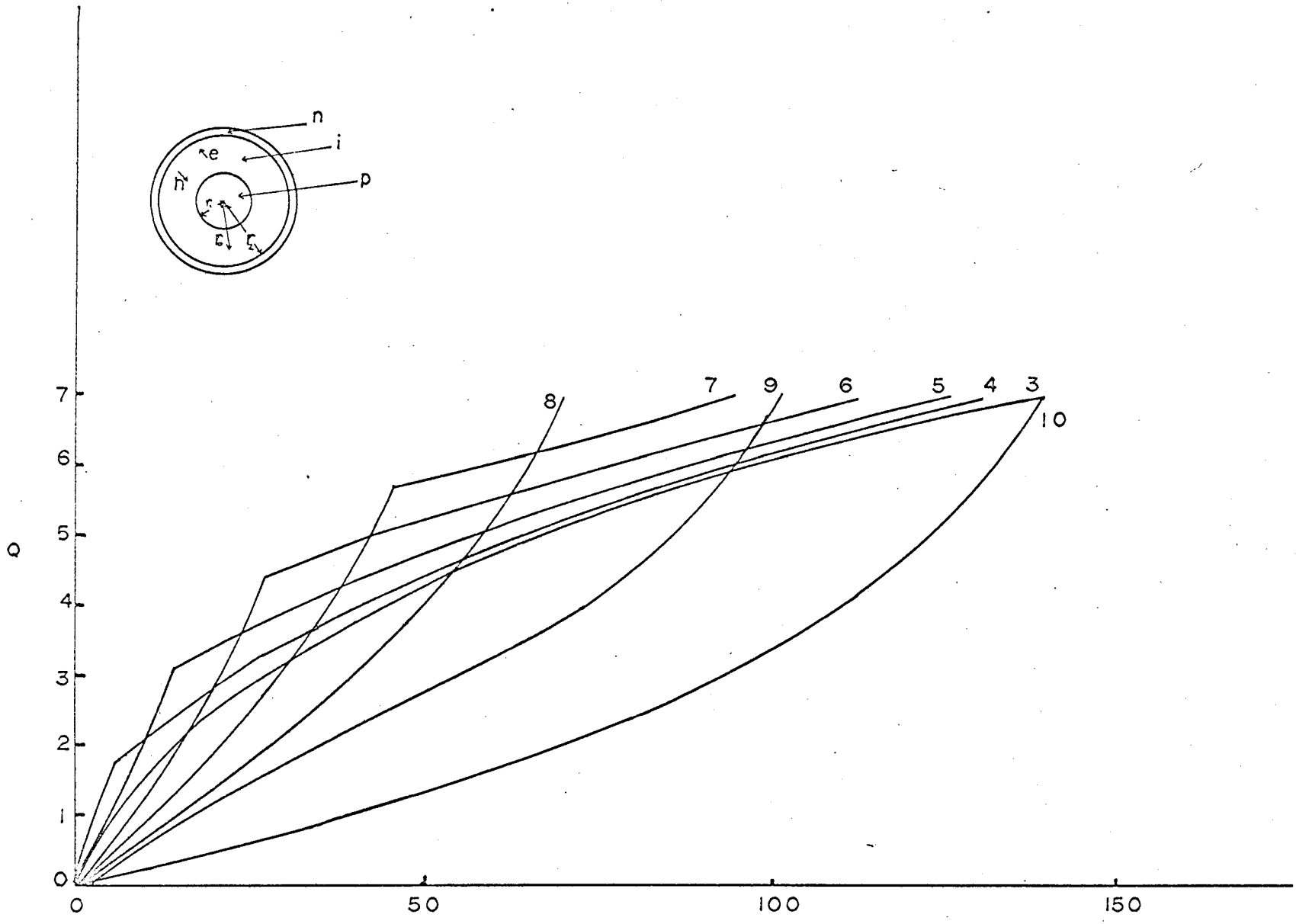

Fig. 3

Pulse shapes in a spherical counter

spherical detector to the pulse shapes of the cylindrical one is obvious. But it can be seen that in all cases the collection times in the spherical counter are almost three times larger than the collection times in the cylindrical detector. Therefore a quantitative comparison of the spherical detector with the cylindrical one is going to show us how much the pulse shapes of the first are slower than the pulse shapes of the second.

2.5 Comparison of the spherical detector to the cylindrical one

Now the two counters cylindrical and spherical are going to be compared quantitatively by plotting the Q against time for the two cases. It is taken $r_1 = 3$ mm and $r_2 = 10$ mm.

We are going to calculate the ratio

$$\frac{(T_{r_1 r_2})^{CYL}}{(T_{r_1 r_2})^{SPH}}$$

where $T_{r_1 r_2}$ is the time that carrier takes to travel across the distance $r_2 - r_1$, i.e. $T_{r_1 r_2}$ = transit time.

(A) Cylindrical Counter

$$E = -\frac{dv}{dr} = \frac{Q}{2\pi\epsilon r} \qquad (23)$$

$$V_{r_1} - V_{r_2} = \frac{Q}{2\pi\epsilon} \ln \frac{r_2}{r_1} = \Delta V \quad . \qquad (24)$$

The drift velocity is given by

$$v = \frac{dr}{dt} = \mu E = \frac{\mu Q}{2\pi\epsilon r} .$$

Integrating from r_1 to r_2 we have

$$\int_{r_1}^{r_2} r dr = \int_{o}^{T_{r_1 r_2}} \frac{\mu Q}{2\pi\epsilon} dt = \frac{\mu Q}{2\pi\epsilon} \int_{o}^{T_{r_1 r_2}} dt \quad . \qquad (25)$$

Substituting Q from (24) into (25) we have:

$$\frac{r_2^2 - r_1^2}{2} = \frac{\mu Q}{2\pi\epsilon} T_{r_1 r_2} = \frac{\mu \Delta V}{\ell n(\frac{r_2}{r_1})} T_{r_1 r_2} .$$

Therefore the transit time is given by

$$(T_{r_1 r_2})^{CYL} = \ell n(\frac{r_2}{r_1}) \frac{(r_2^2 - r_1^2)}{2\mu\Delta V}$$

when the ionization occurs at $r_o = \bar{r}_o = (\frac{r_1^2 + r_2^2}{2})^{\frac{1}{2}} = 7.4$ mm the collection times are equal.

(B) Spherical Counter

$$E = - \frac{dv}{dr} = \frac{Q}{4\pi\epsilon r^2}$$

$$V_{r_1} - V_{r_2} = \frac{(r_2 - r_1)}{4\pi\epsilon r_1 r_2} Q = \Delta V. \qquad (26)$$

The equation of motion is

$$v = \frac{dr}{dt} = \mu E = \frac{\mu Q}{4\pi\epsilon r^2} .$$

From integrating from r_1 to r_2 we have

$$\int_{r_1}^{r_2} r^2 dr = \frac{\mu Q}{4\pi\varepsilon} \int_{o}^{T_{r_1 r_2}} dt \qquad (27)$$

where $T_{r_1 r_2}$ is the transit time.

$$\frac{1}{3}(r_2^3 - r_1^3) = \frac{\mu Q}{4\pi\varepsilon} T_{r_1 r_2} = \frac{r_1 r_2}{(r_2 - r_1)} \mu \Delta V T_{r_1 r_2} \quad . (28)$$

Therefore the transit time in the case of a spherical counter is given by

$$(T_{r_1 r_2})^{SPH} = \frac{(r_2^3 - r_1^3)(r_2 - r_1)}{3 r_1 r_2 \mu \Delta V} \quad . \qquad (29)$$

When the ionization occurs at

$$r_o = \bar{r}_o = \left(\frac{r_1^3 + r_2^3}{2}\right)^{1/3} = 7.92$$

the collection times are equal.

Taking the ratio

$$\frac{(T_{r_1 r_2})^{CYL}}{(T_{r_1 r_2})^{SPH}}$$

we have

$$\frac{(T_{r_1 r_2})^{CYL}}{(T_{r_1 r_2})^{SPH}} = \frac{3}{2} \frac{r_1 r_2 \, \ell n(\frac{r_2}{r_1})}{r_1^2 + r_1 r_2 + r_2^2} \quad . \qquad (30)$$

Because of $r_1 = 3$ mm, $r_2 = 10$ mm (30) gives

$$\frac{(T_{r_1 r_2})^{CYL}}{(T_{r_1 r_2})^{SPH}} = \frac{54}{139} \quad . \qquad (31)$$

It can be seen from this relation that the transit time in the spherical counter is almost 3 times longer than the transit time in the cylindrical counter. In our case we have a coaxial counter which is a mixture of cylindrical and spherical counter (Figure (1)). Normally the spherical portion contributes more than half interaction. So in timing measurements with short coaxial diodes limitations have been found in the coincidence resolving times due to large variations in charge collection times which result from the non-uniformity of the electric field - especially in the spherical portion. We can improve the electric field uniformity making longer coaxial diodes. So in this case the cylindrical part of the detector is expanded.

2.6 Time distribution for collection of specific amount of charge $\tilde{Q}$

The time required to collect a specific amount, a fraction, of charge, depends upon the point of charge creation r_o. Thus if we let $t_Q(r_o)$ be this time, we wish to calculate the distribution

$$P(t_Q)dt_Q = P(r_o(t_Q)] \frac{dr_o}{dt_Q} dt_Q.$$

The relation $r_o(t_Q)$ is derived from the equation for the charge pulse. The distribution in r_o is based upon geometrical considerations. The probability of an interaction is proportional

to the volume element defined by the limits $r_o \rightarrow r_o + dr_o$. For axial symmetry, per unit length, we have

$$P(r_o)dr_o = 2\pi r_o dr_o$$

while for spherical symmetry

$$P(r_o)dr_o = 4\pi r_o^2 dr_o.$$

The calculation for the case of spherical symmetry is not tractable analytically and will not be discussed further here.

It is now necessary to decompose the charge collection process into three distinctive cases. These three cases are:

(a) The charge Q arises from partial integration of both electron and hole currents, $Q<Q_1$ or Q_2.

(b) The charge Q arises from complete integration of the electron current, and partial integration of the hole current $Q_1<Q<Q_1+Q_2$.

(c) The charge Q arises from complete integration of the hole current, and partial integration of the electron current.

These three cases correspond to initial charge creation in three distinct regions of the counter, designated r_o belongs to A(Q), B(Q) or C(Q) respectively. Qualitatively, when r_o lies near the center of counter electrodes, it is necessary to collect both electron and hole currents to accumulate the charge Q. When r_o lies near the n-type junction, it is necessary to collect all the electron

current, and part of the hole current to accumulate the charge Q. When r_o lines near the p-type junction the converse is true.

The three regions may be described by the limits

r_o belongs to A when $R_1 < r_o < R_2$

r_o belongs to B when $r_1 < r_o < R_1$

r_o belongs to C when $R_2 < r_o < r_1$

1. Both components are contributing

We consider first the case where both components are contributing, so we have:

$$\tilde{Q} = \tilde{Q}_1 + \tilde{Q}_2 = (r_o^2 + t)^{\frac{1}{2}} - (r_o^2 - t)^{\frac{1}{2}}$$

or

$$[\tilde{Q} + (r_o^2 - t)^{\frac{1}{2}}]^{\frac{1}{2}} = r_o^2 + t = \tilde{Q}^2 + r_o^2 - t + 2\tilde{Q}(r_o^2 - t)^{\frac{1}{2}}.$$

Solving respect to t we take

$$t = \tilde{Q}(r_o^2 - \frac{\tilde{Q}^2}{4})^{\frac{1}{2}} \text{ where } 0 \leq t \leq r_o^2 - r_1^2 \qquad (32)$$

Q_1 ENDS FIRST , $r_o < \bar{r}_o = \left(\frac{r_1^2 + r_2^2}{2}\right)^{\frac{1}{2}}$

The total $\tilde{Q}$ in this case:

$$\tilde{Q} = (r_o^2 + t)^{\frac{1}{2}} - r_1 \text{ where } r_o^2 - r_1^2 \leq t \leq r_2^2 - r_o^2 \ . \quad (33)$$

Solving respect to t we get

$$t = (\tilde{Q} + r_1)^2 - r_o^2 \ , \ r_o^2 - r_1^2 \leq t \leq r_2^2 - r_o^2 \ . \quad (34)$$

Now let us find the value of r_o which gives straight line to $\tilde{Q}$ i.e. both components. The relation $t = (\tilde{Q} + r_1)^2 - r_o^2$ holds starting at $t = r_o^2 - r_1^2$.

So $$r_o^2 - r_1^2 = (\tilde{Q} + r_1)^2 - r_o^2$$

or $$Z^2 = r_o^2 = \frac{1}{2}(\tilde{Q}^2 + 2\tilde{Q}r_1 + 2r_1^2) \ . \quad (35)$$

So Z is the value of r_o which will give both components up to just $\tilde{Q}$ i.e. smallest r_o. The largest r_o is $\bar{r}_o^2 = \frac{r_1^2 + r_2^2}{2}$.

Therefore the limits of r_o are:

$$Z \leq r_o \leq \bar{r}_o \ .$$

Now let us find the time limits.

(a) Shortest time

We substitute in (32) the relation (35).

Therefore $$t_s = \tilde{Q}(r_o^2 - \frac{\tilde{Q}^2}{4})^{\frac{1}{2}} = \tilde{Q}(\frac{\tilde{Q}^2}{4} + r_1\tilde{Q} + r_1^2)^{\frac{1}{2}} \ .$$

(b) Longest time

We substitute in (32) the relation $\bar{r}_o^2 = \frac{r_1^2 + r_2^2}{2}$

So we have $$t_L = \tilde{Q}(r_o^2 - \frac{\tilde{Q}^2}{4})^{\frac{1}{2}} = \tilde{Q}(\frac{r_1^2 + r_2^2}{2} - \frac{\tilde{Q}^2}{4})^{\frac{1}{2}}$$

Therefore the time limits are:

$$\tilde{Q}(\frac{\tilde{Q}}{4} + r_1\tilde{Q} + r_1^2)^{\frac{1}{2}} \leq t \leq \tilde{Q}(\frac{r_1^2 + r_2^2}{2} - \frac{\tilde{Q}^2}{4})^{\frac{1}{2}} \qquad (36)$$

or $$t_1 \leq t \leq t_2 \ .$$

Weighting for r_o is $P(r_o) = r_o$.

From $$t = \tilde{Q}(r_o^2 - \frac{\tilde{Q}^2}{4})^{\frac{1}{2}}$$

we have $$P(t) = P(r_o)\frac{dr_o}{dt} = \frac{r_o}{\tilde{Q}r_o}(r_o^2 - \frac{\tilde{Q}}{4})^{\frac{1}{2}} = \frac{t}{\tilde{Q}^2}$$

or $$P(t) = \frac{t}{\tilde{Q}^2} \ .$$

Q_2 ENDS FIRST $\qquad r_o > \bar{r}_o = (\frac{r_1^2 + r_2^2}{2})^{\frac{1}{2}}$

In this case the total $\tilde{Q}$ is

$$\tilde{Q} = r_2 - (r_o^2 - t)^{\frac{1}{2}} \text{ where } r_2^2 - r_o^2 < t < r_o^2 - r_1^2 \ .$$

Solving respect to t we have:

$$t = r_o^2 - (\tilde{Q} - r_2)^2 \quad r_2^2 - r_o^2 \leq t \leq r_o^2 - r_1^2. \qquad (37)$$

The limits of r_o are

$$t = \tilde{Q}(r_o^2 - \frac{\tilde{Q}^2}{4})^{\frac{1}{2}} \quad \text{where} \quad 0 \leq t \leq r_2^2 - r_o^2$$

if we substitute $t = r_2^2 - r_o^2$ in (37) we take

$$r_2^2 - r_o^2 = r_o^2 - (\tilde{Q} - r_2)^2$$

or

$$r_o^2 = \frac{\tilde{Q}^2}{2} - r_2\tilde{Q} + r_2^2 = K \quad . \tag{38}$$

So the limiting values of r_o are K and $\bar{r}_o$

$$\bar{r}_o \leq r_o \leq K$$

or

$$\frac{r_1^2 + r_2^2}{2} \leq r_o^2 = \leq \frac{\tilde{Q}^2}{2} - r_2\tilde{Q} + r_2^2$$

Time Limits

We substitute in eqn (32) the relation $r_o^2 = \frac{r_1^2 + r_2^2}{2}$

(a) Shortest time

$$t_s = \tilde{Q}(r_o^2 - \frac{\tilde{Q}^2}{4}) = \tilde{Q}(\frac{r_1^2 + r_2^2}{2} - \frac{\tilde{Q}^2}{4})^{\frac{1}{2}}$$

(b) Longest time

We substitute in eqn (32) the eqn (38).

Therefore

$$t_L = \tilde{Q}(r_o^2 - \frac{\tilde{Q}^2}{4})^{\frac{1}{2}} = \tilde{Q}(\frac{\tilde{Q}^2}{4} - r_2\tilde{Q} + r_2^2)^{\frac{1}{2}} \quad .$$

So the time limits are:

$$\tilde{Q}(\frac{r_1^2+r_2^2}{2} - \frac{\tilde{Q}^2}{4})^{\frac{1}{2}} \leq t \leq \tilde{Q}(\frac{\tilde{Q}^2}{4} - r_2\tilde{Q} + r_2^2)^{\frac{1}{2}} \tag{39}$$

or

$$t_2 \leq t \leq t_4 .$$

From the relations (36) and (39) we find the final limits

$$\tilde{Q}(\frac{\tilde{Q}^2}{4} + r_1\tilde{Q} + r_1^2)^{\frac{1}{2}} \leq t \leq \tilde{Q}(\frac{\tilde{Q}^2}{4} - r_2\tilde{Q} + r_2^2)^{\frac{1}{2}} \tag{40}$$

or

$$t_1 \leq t \leq t_4 \quad .$$

2. One component is contributing (electrons)

For the case where $r_o < \bar{r}_o$ we use $t = (\tilde{Q} + r_1)^2 - r_o^2$ (41)

if $r_o = r_1$ the charge collection is due only to electrons and

$$t_3 = \tilde{Q}^2 + 2r_1\tilde{Q} \qquad (41)$$

$$P(t) = P(r_o)\frac{dr_o}{dt}$$

In this case $P(t) = \frac{1}{2}$.

3. One component is contributing (holes)

For the case where $r_o > \bar{r}_o$ we use $t = r_o^2 - (\tilde{Q} - r_2)^2$

When $r_o = r_2$ the charge collection is due only to holes and the time is

$$t_5 = 2\tilde{Q}r_2 - \tilde{Q}^2 \qquad (42)$$

Also in this case $P(t) = \frac{1}{2}$.

Therefore if any particular $\tilde{Q}$ is selected (Q_{max} is constant) the time distribution is

$$P(t) = \frac{t}{\tilde{Q}^2}$$

for the case where both components are contributing, and

$$P(t) = \frac{1}{2}$$

for the case where only one component is contributing.

The maximum charge is

$$Q_{max} = r_2 - r_1.$$

The time limits are

$$\begin{aligned} t_1 &= \tilde{Q}\left(\frac{\tilde{Q}^2}{4} + r_1\tilde{Q} + r_1^2\right)^{\frac{1}{2}} \\ t_2 &= \tilde{Q}\left(\frac{r_1^2 + r_2^2}{2} - \frac{\tilde{Q}^2}{4}\right)^{\frac{1}{2}} \\ t_3 &= \tilde{Q}^2 + 2r_1\tilde{Q} \\ t_4 &= \tilde{Q}\left(\frac{\tilde{Q}^2}{4} - r_2\tilde{Q} + r_2^2\right)^{\frac{1}{2}} \\ t_5 &= 2r_2\tilde{Q} - \tilde{Q}^2 \end{aligned} \qquad (43)$$

Schematically these results are shown in Figure (4). Effects not included are finite range, noise and jitter in trigger level of timing circuits. These if included would have the effect of smoothing the illustrated curves with a Gaussian.

If $t_3 < t_2$ indicates that the component B does not exist, because all charge is collected before $\tilde{Q}$ is reached. If $t_4 < t_3$ indicates that the component C does not exist.

2.7 Calculated case

We take $r_1 = 3$ mm, $r_2 = 10$ mm.

The maximum charge is

$$Q_{max} = r_2 - r_1 = 7.$$

We are going to trigger at $\frac{1}{7}$, $\frac{3}{7}$, $\frac{5}{7}$ of total charge.

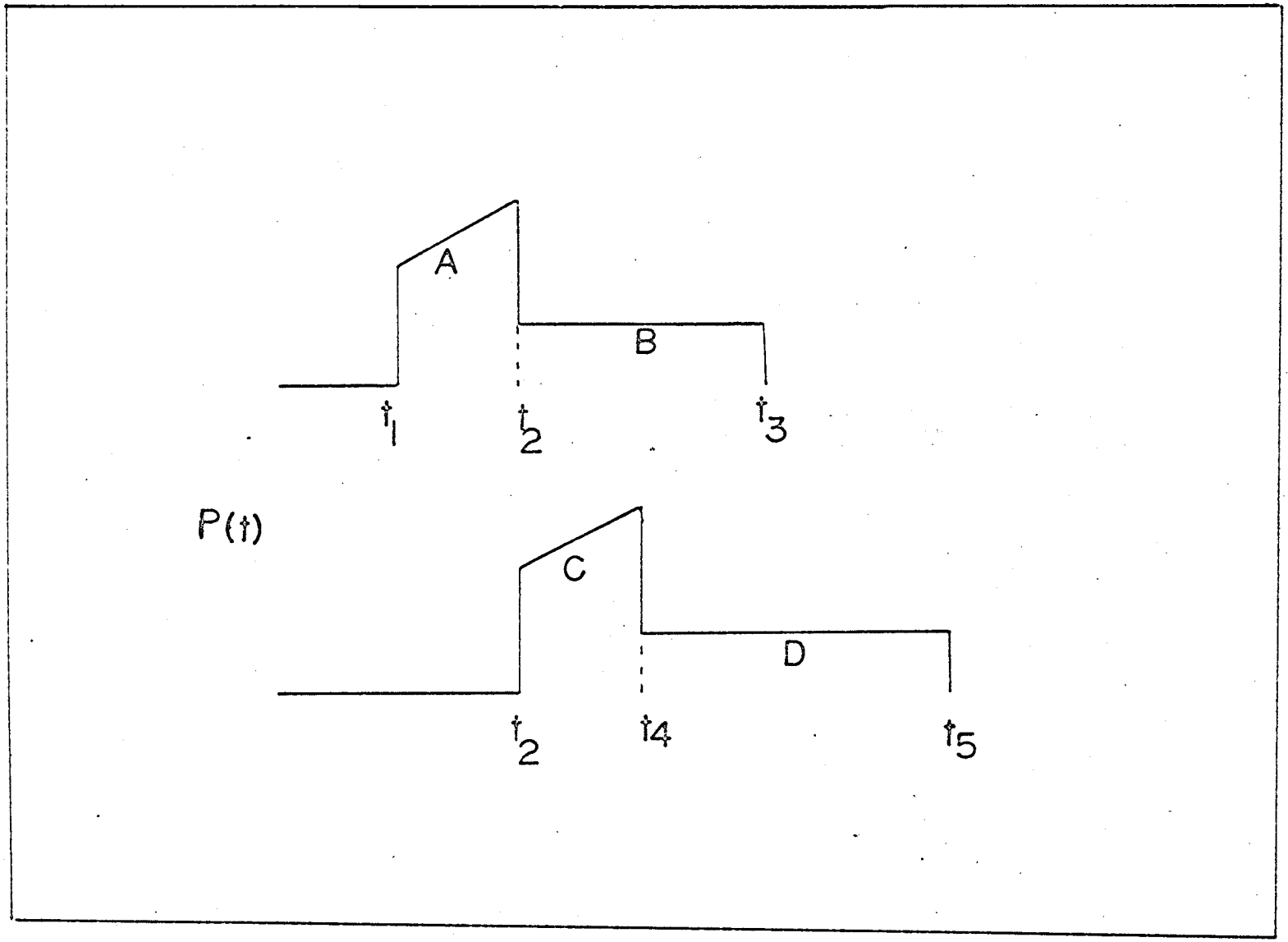

Fig. 4 Time distribution for collection of charge $\tilde{Q}$

1. $\tilde{Q} = 1$

We substitute the values of r_1, r_2 and $\tilde{Q}$ in relations (43) and we find the time limits.

$$t_1 = \tilde{Q}\left(\frac{\tilde{Q}^2}{4} + r_1\tilde{Q} + r_1^2\right)^{\frac{1}{2}} = 3.5 \text{ nsec}$$

$$t_2 = \tilde{Q}\left(\frac{r_1^2 + r_2^2}{2} - \frac{\tilde{Q}^2}{4}\right)^{\frac{1}{2}} = 7.4 \text{ nsec}$$

$$t_3 = \tilde{Q}^2 + 2r_1\tilde{Q} = 7 \text{ nsec}$$

$$t_4 = \tilde{Q}\left(\frac{\tilde{Q}^2}{4} - r_2\tilde{Q} + r_2^2\right)^{\frac{1}{2}} = 9.5 \text{ nsec}$$

$$t_5 = 2r_2\tilde{Q} - \tilde{Q}^2 = 19 \text{ nsec.}$$

It can be seen that $t_3 < t_2$ therefore component B does not exist, also $t_4 < t_3$ therefore component C does not exist. The intensities are

$$P(t_1) = \frac{t_1}{\tilde{Q}^2} = 3.5$$

$$P(t_4) = \frac{t_4}{\tilde{Q}^2} = 9.5 \ .$$

For the case where only one component contributes $P(t) = 0.5$. Using these results the time distribution at a triggering level $\frac{1}{7}$ has been plotted in Figure (5).

2. $\tilde{Q} = 3$

For this case the time limits are

$$t_1 = 13.5 \text{ nsec}$$

$$t_2 = 21.5 \text{ nsec}$$

$t_3 = 27$ nsec

$t_4 = 22.5$ nsec

$t_5 = 51$ nsec.

$t_4 < t_3$ therefore component C (Figure (4)) does not exist.

The intensities are

$P(t_1) = 1.5$

$P(t_2) = 2.4$, $P(t) = 2.4 + 0.5 = 2.9$

$P(t_3) = 3$

$P(t_4) = 2.8$, $P(t) = 2.8 + 0.5 = 3.3$

(Figure (5)).

3. $\tilde{Q}=5$

The time limits are

$t_1 = 27.5$ nsec

$t_2 = 34.5$ nsec

$t_3 = 55$ nsec

$t_4 = 37.5$ nsec

$t_5 = 75$ nsec

$t_4 < t_3$ therefore component C (Figure (4)) does not exist.

The intensities are

$P(t_1) = 1.1$

$P(t_2) = 1.3$, $P(t) = 1.3 + 0.5 = 1.8$

$P(t_4) = 1.5$, $P(t) = 1.5 + 0.5 = 2.$

The results of these calculations have been plotted in Figure (5). Effects like finite range, noise and jitter in trigger level of timing circuits are not included.

Fig. 5 Time distribution for Q = 1/7, Q = 3/7, Q = 5/7

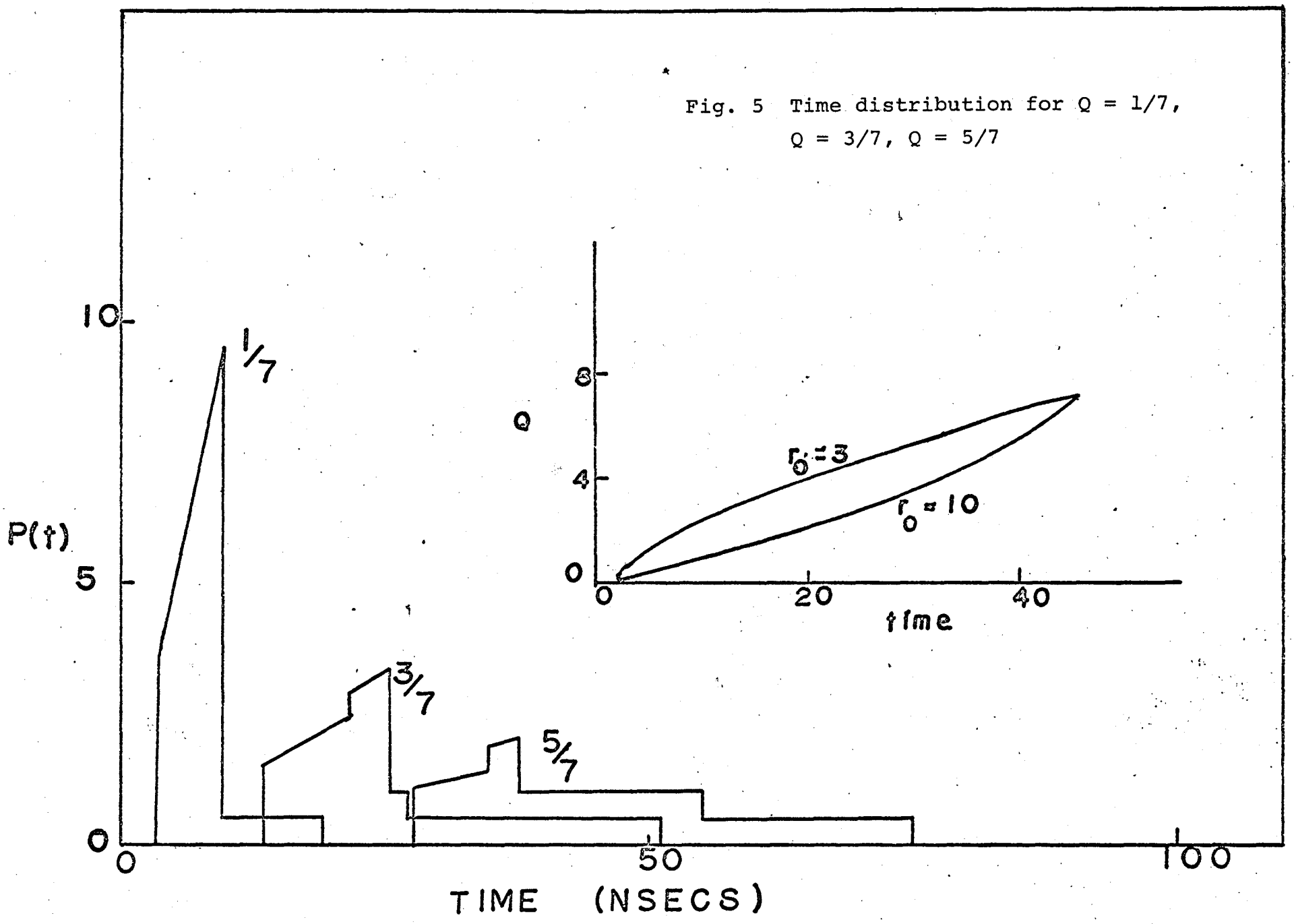

CHAPTER III

EXPERIMENTAL TECHNIQUES

3.1 Study of ^{24}Na

Figure (6) illustrates in block diagram form the typical experimental arrangement employed for timing studies using a Ge(Li) counter and a plastic scintillator. A leading edge trigger circuit was used (ORTEC Time Pickoff) for the Ge(Li) device which may be set to trigger at a small fraction of the total charge. Since Ge(Li) detectors characteristically have long collection time (> 30 nsec) and energy resolution is of the utmost importance, the time pickoff should be connected between the preamplifier and the shaping amplifier, where signal to noise ratio will not be appreciably affected.

In a γ-γ coincidence arrangement for which ^{24}Na was studied we used a plastic scintillation counter (NE102) and a 18 cm^3 Ge(Li-drift) coaxial detector. The surface of the counter was 12 cm^2, the height was 1.4-1.6 cm and the active volume was about 15 cm^3 as determined by copper staining. The radiant energy from the source was uncollimated, so that the pulses were given by collection from all parts of the detector.

The pulses from the time-to-amplitude converter pass into a multichannel pulse-height-analyzer. The time-to-amp-

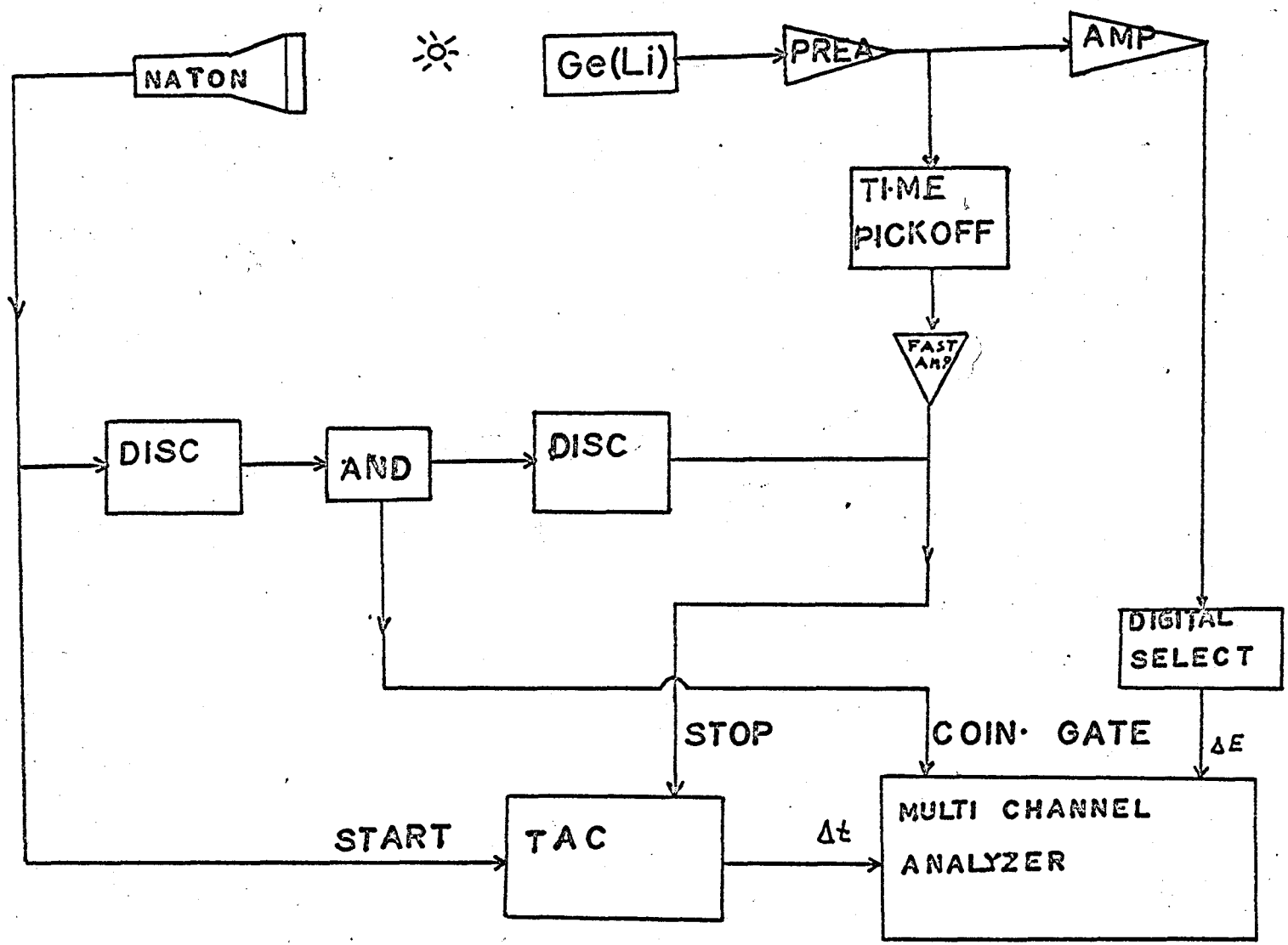

Fig. 6 Block diagram of a γ-γ coincidence experiment

litude converter converts the time difference between two pulses into a signal whose amplitude depends upon this difference. The time differences are accumulated in the multichannel analyzer and the distribution of this quantity is thus sampled. The linear gate was controlled by a single-channel differential pulse-height analyzer whose window was adjusted to cover the desired range of energy as well as a "fast" coincidence condition.

For this experiment 512 channels were required in the time dimension and 1024 channels on the Ge(Li) dimension in order to retain sufficient resolution. This requires 2^{19} ($\sim$ 500,000) memory locations to record the information in real time. Since such size random access memories are not available delayed time analysis was used in order to record the entire coincidence surface concurrently. The addresses were stored on a magnetic tape and later these addresses were sorted.

When the data was sorted from the magnetic tape into the analyzer, the analyzer memory was divided into a rectangular array with 64 channels in the x-dimension which were arranged to span the pulse height spectrum of the time distribution of interest. So in the above array there are $64 \times 256 = 16,355$ available channels for storage of counts. The total data will form a three dimensional surface, where

the z-dimension is the number of counts in the channel. Four such scans of the recorded data were conducted to provide a 64×1024 channel surface.

3.2 Study of ^{22}Na

Another experiment was done using the positron emitter ^{22}Na as a source in order to enhance the data acquisition rate. a total of seven runs were done where appried bias voltage effects were studied. The analyzer memory was divided into a rectangular array with 256 channels in the x-dimension (time) and 64 channels in the y-dimension (energy). Using a gain of $\sim$ 1 keV/channel digital windows were set in order that the 511-keV photopeak was centered in the 64 channels assigned to the energy dimension.

Figure (7) is the block diagram of an experiment in which the pulse shapes from a Ge(Li) detector were studied. The source was again ^{22}Na. A plastic scintillator was used to trigger a Philips sampling oscilloscope which monitored pulses from the Ge(Li) counter. Pulse height analysis of the x and y oscilloscope outputs permitted one to accumulate a pulse distribution.

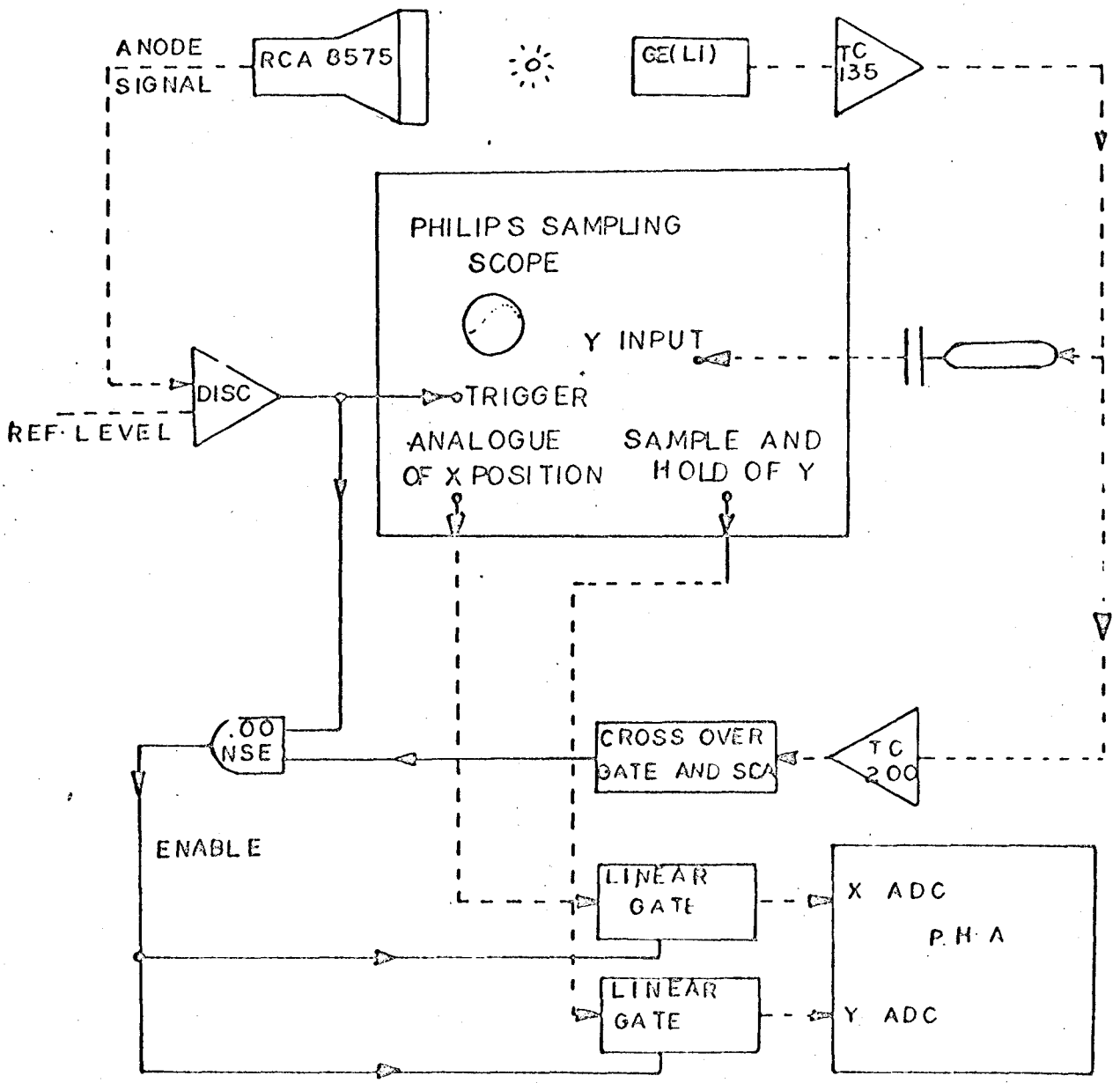

Fig. 7

Block diagram for the study of pulse shapes of ^{22}Na

CHAPTER IV

ANALYSIS OF COINCIDENCE DATA

4.1 Study of ^{24}Na

A coincidence experiment was conducted using a ^{24}Na source. The coincident information of interest i.e. the energy recorded in the Ge(Li) parameter and the time difference between the Ge(Li) and plastic counters, was encoded and stored on magnetic tape in the form of paired addresses. The energy range covered by the Ge(Li) counter was from 0 to 3000 keV and the time range from 0 to 8 nsec. Initially it was of interest to examine the general nature of the walk function and for this the data was sorted on a coarse mesh. The energy parameter was gathered into 1024 channels from a recorded field of 4096 channels. The time mesh was compressed from 4096 channels to 512 and the 64 channels covering the prompt curve were sorted. The chance contribution was obtained by sorting a second 64 channel region well delayed from the prompt peak.

Figure (8) illustrates an example of a time curve. The figure shows a distribution having a prompt component on the leading edge and a slowly decaying component at later times. In addition a constant component from chance events

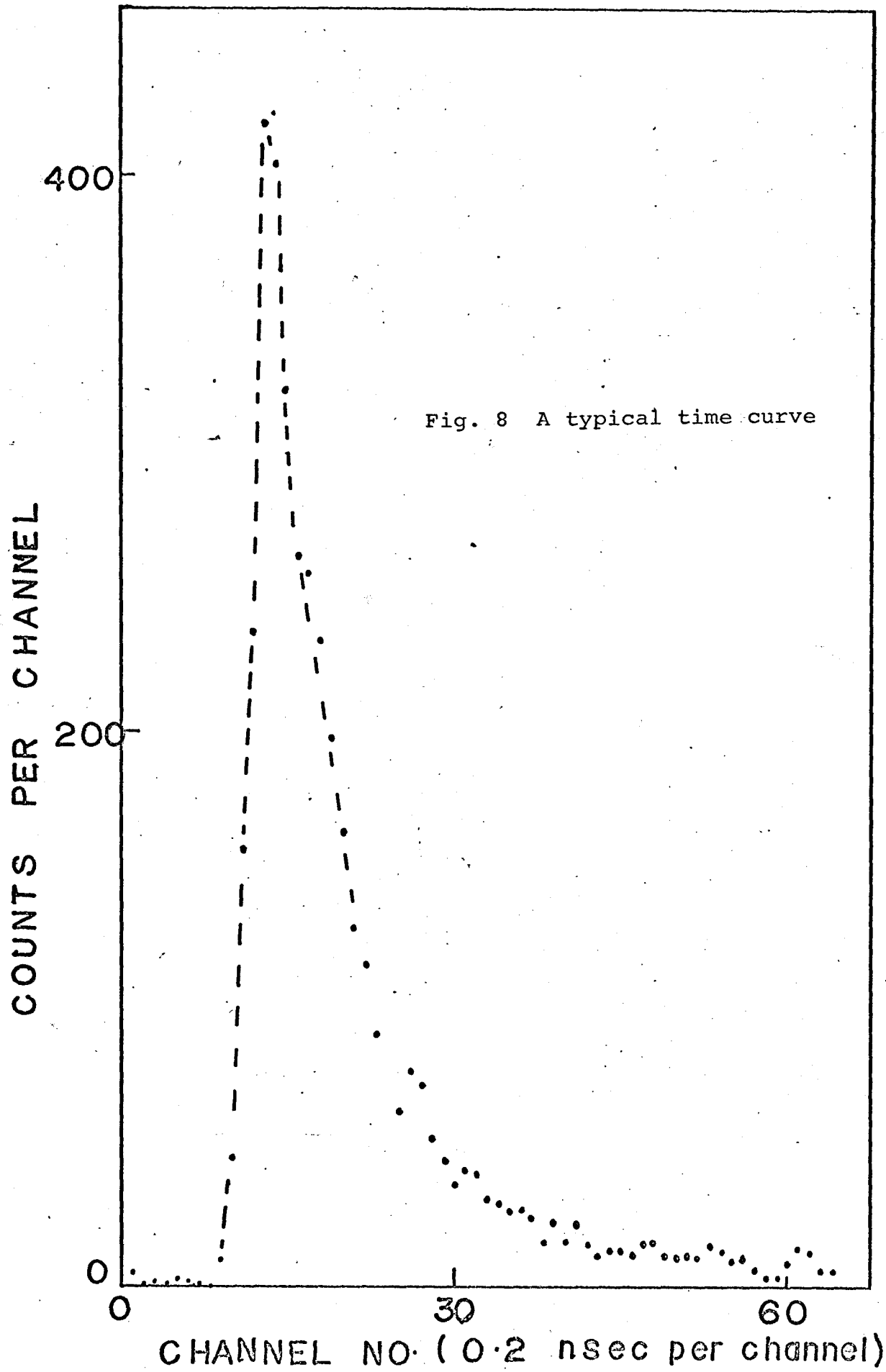

Fig. 8 A typical time curve

is also present. All the time distribution curves from this experiment had assymetrical shapes with exponential tails. These tails were due to low collection fields in the corners of the detector. The walk function was determined by obtaining the centroid of the 1024 time curves of which one is illustrated in Figure (8). The coincidence of unrelated events (chance) has to be taken into consideration because it affects the position of the centroid, so a correction for the chance component was made and the results are shown graphically in figure (9b).

The hyperbolic nature of the walk curve is apparent in figure (9 b) . Since the trigger circuit is probably a function of both input voltage and rate of change of input voltage one would expect that the product of energy times time delay is constant i.e.

$$Et \sim \text{constant}$$

In order to examine this model the product Et was computed. Since time zero is not known we have $E(t-t_o) \sim$ constant, hence the product should give a straight line when plotted against E. This result is shown in Figure (9c) where it is seen that the model is reasonably accurate.

Examination of the walk curve in Figure (9c) reveals large excursions of the curve in the region where peaks occur in the pulse height spectrum. The nature of the deviations

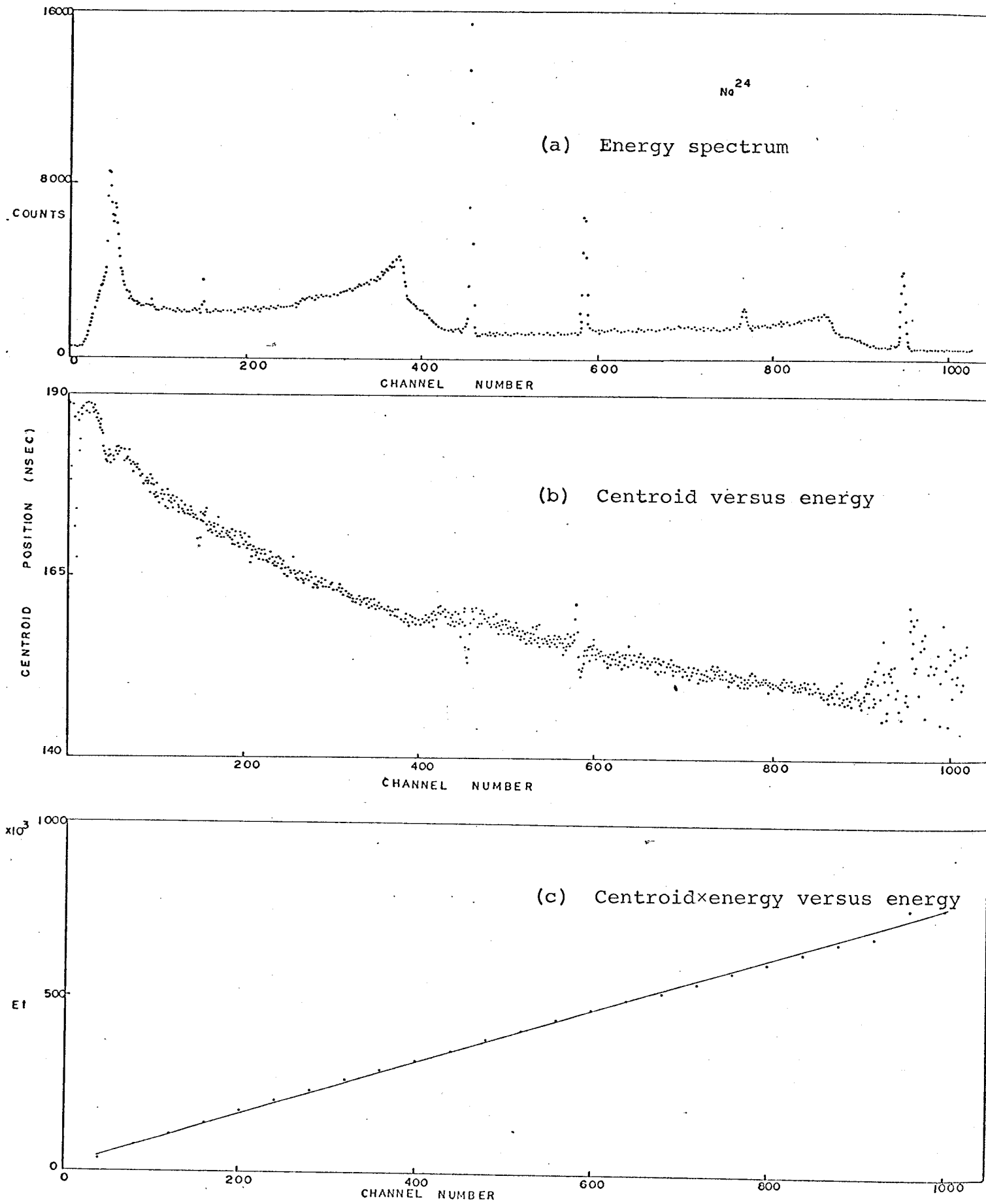
Na24
(a) Energy spectrum
16000
8000
0
COUNTS
0
200
400
600
800
1000
CHANNEL NUMBER
(b) Centroid versus energy
190
165
140
CENTROID POSITION (NSEC)
200
400
600
800
1000
CHANNEL NUMBER
(c) Centroid×energy versus energy
x10^3
1000
500
0
Et
200
400
600
800
1000
CHANNEL NUMBER

Fig. 9

in time centroid indicates that early timing is correlated with increased energy. Since all peaks reveal these centroid excursions it seemed advantageous to examine this effect in more detail. Since a source with two coincident γ-rays is required for timing studies a very suitable source is ^{22}Na, a positron emitter, which gives two γ-rays at 180° with respect to each other, each with E_γ = 511 keV. The high counting efficiency obtainable with such a source makes the following studies quite feasible.

4.2 Study of Dependence of Pulse Shape and Time Distribution Upon Voltage

A coincidence experiment was conducted using a ^{22}Na source. In these measurements the ^{22}Na source was used between a plastic detector and a Ge(Li) detector. Various runs were done changing in every run the voltage on the Ge(Li) counter. The energy parameter of the Ge(Li) counter was recorded into 64 channels for a recorded field of 4096 channels and covered the 511 keV photopeak. The time was compressed from 4096 channels to 512 of which 256 channels were recorded.

Figure (10) shows the observed time distributions as a function of bias voltage for constant energy. The energy selected in each case corresponded to the centroid of the 511 keV photopeak. As the voltage is increased from 310 v to 1600 v the curves sharpen and the peak position moves over towards the start pulse. As the bias is decreased the rise time of the

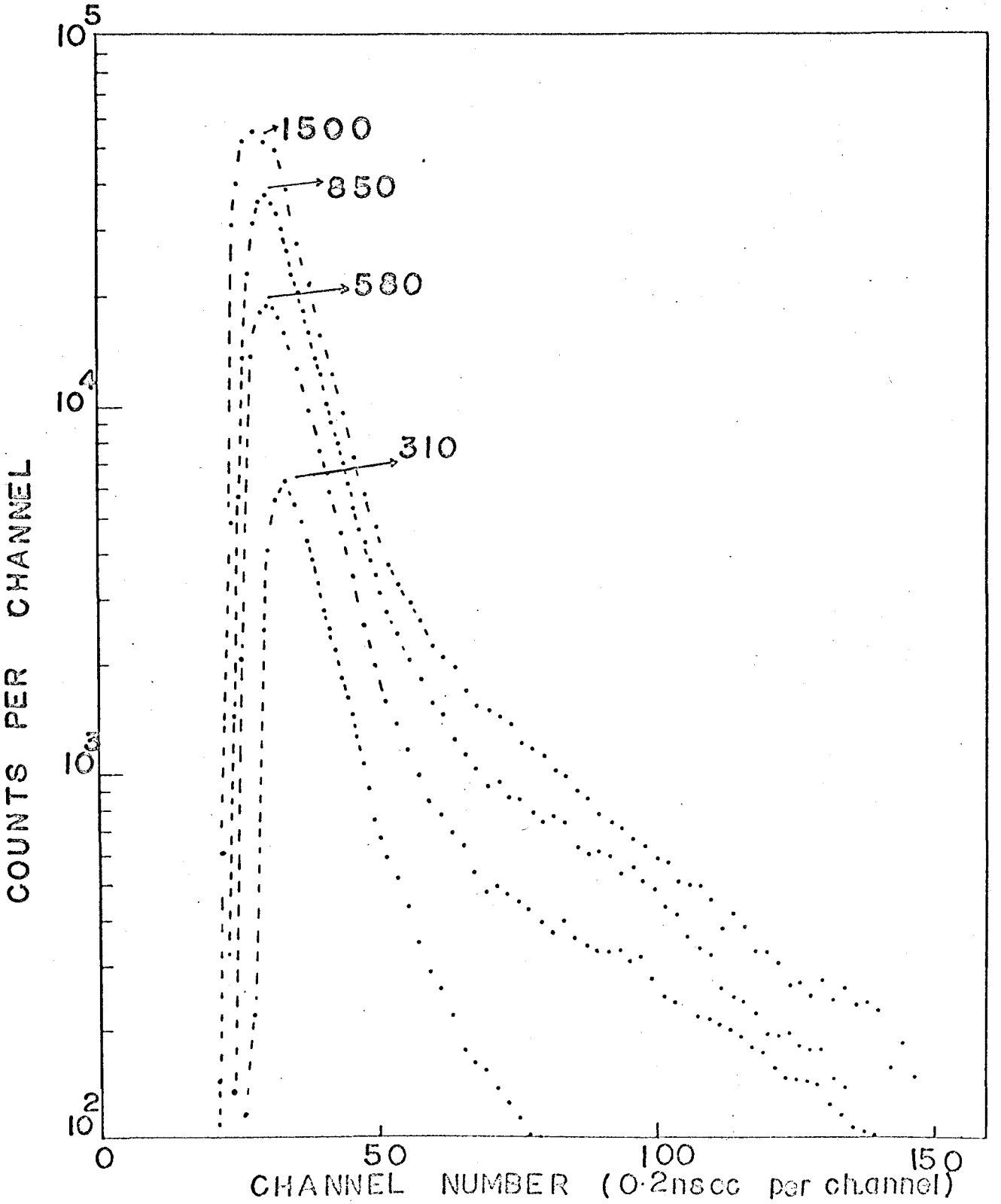

Fig. 10

Time distributions for various bias voltages

time distribution curves or the charge collection time is increased. The spread also in rise time is increased with decreased voltage. Rise time variations also affect the energy resolution as we will see shortly.

Figure (11) illustrates four energy distribution curves at different times. These distributions look like Gaussians with a linear background. The background of course has to be subtracted. We used the following method. From the 256 energy spectra the one with the most counts was selected and a background was made up. So according to this, the background of the remaining 255 spectra was found. The next step was to subtract the background from the spectra. This work was done for all the seven 16K spectra corresponding to the different detector biases. From the Figure (11) it can be seen that the position of the centroid changes as the time increases. Also it is evident that the peak gets broader with time. A better illustration of this change can be seen in Figure (12) which shows the projection of energy spectra on the time axis, i.e. the amplitude. This figure shows three distributions with various voltages. It can be seen that as the voltage increases the quasi-flat region disappears.

From these time distributions the rise time can be defined as the time between the 10 percent and the 90 percent

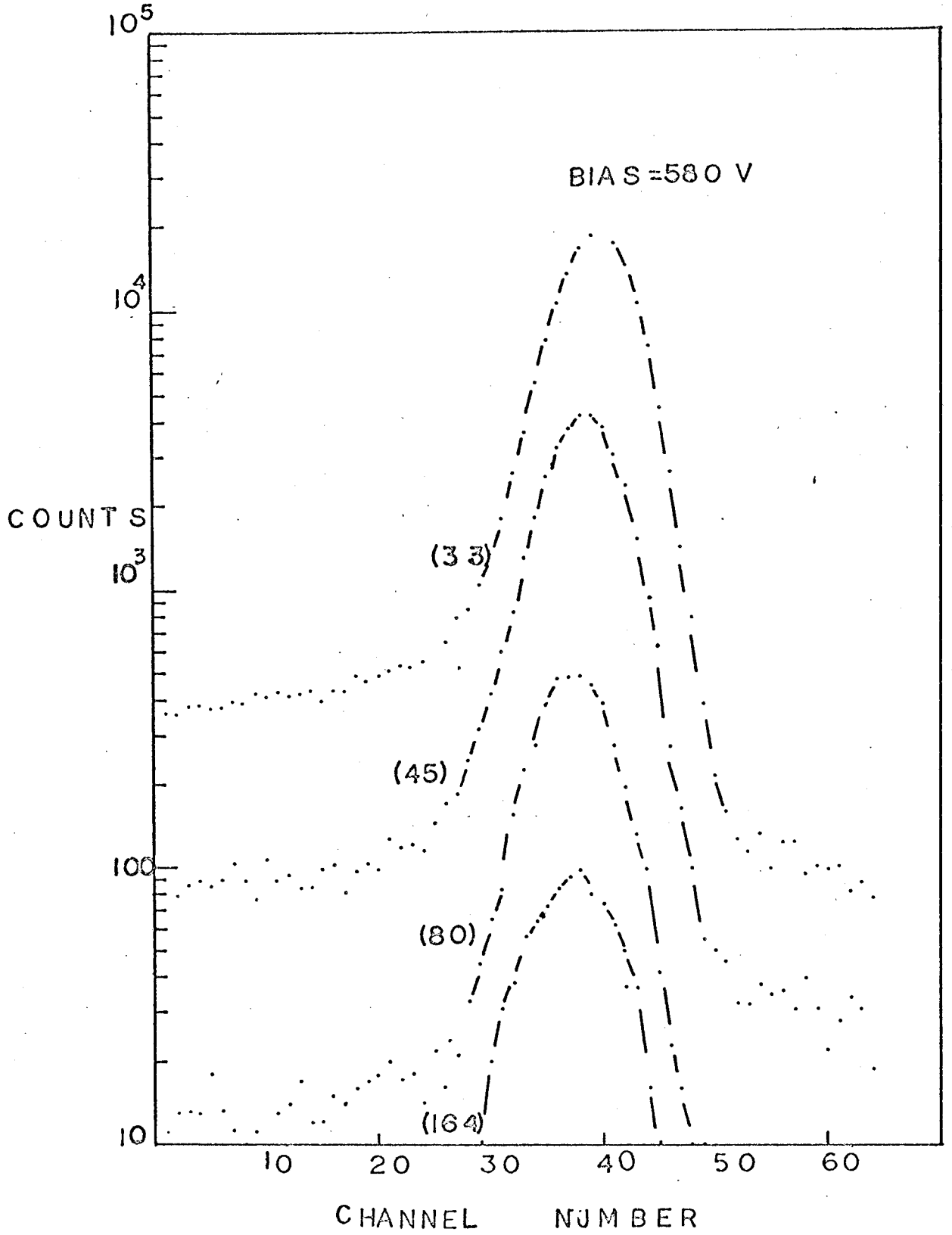

Fig. 11

Energy distributions for various times

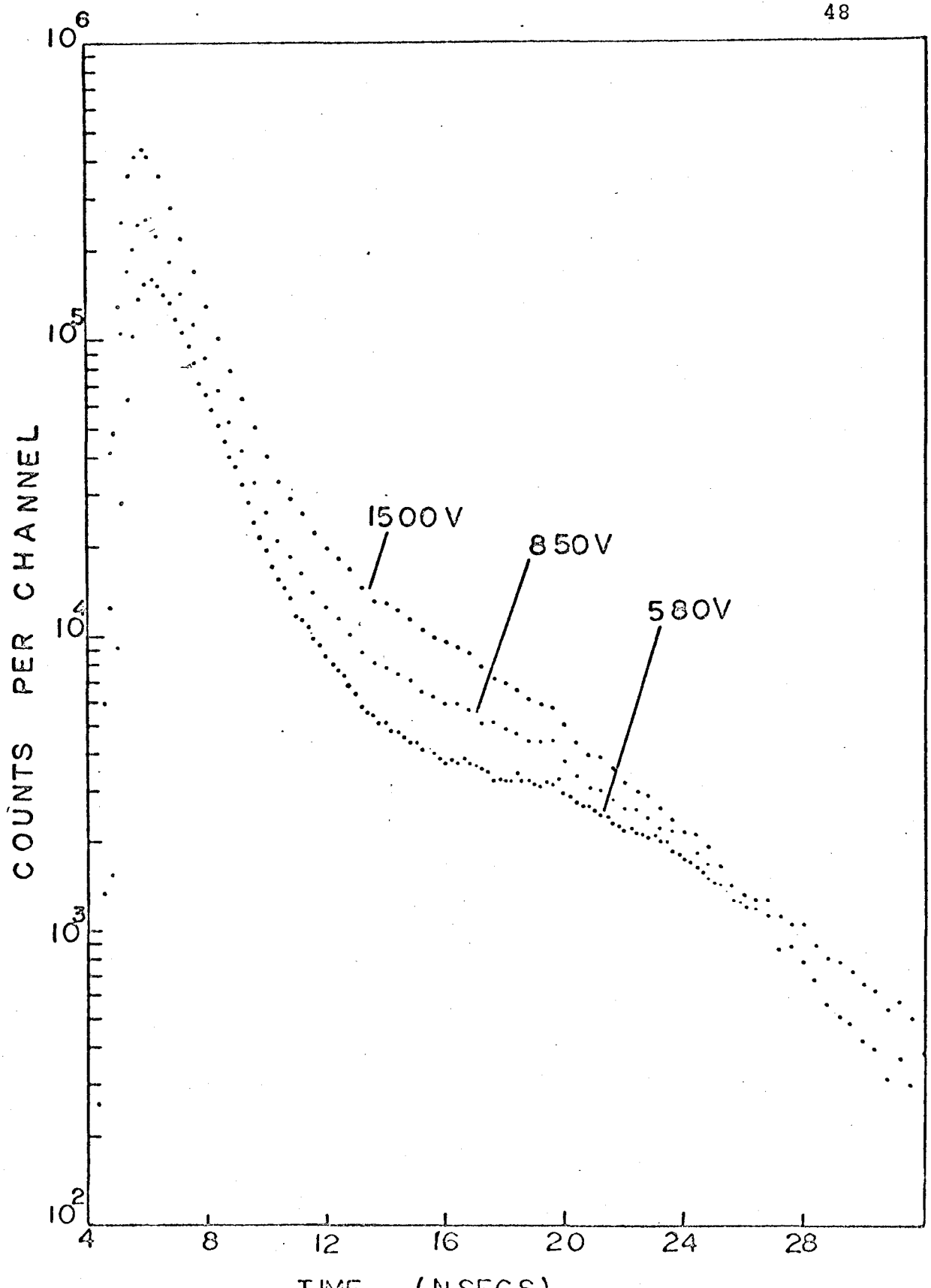

Fig. 12

Projection of energy distributions on time axis

of the peak if we consider the highest point of the curve as the 100 percentpoint. It is known that the rise time is a step function convoluted with a Gaussian function. So now we take the differences between the successive points of the rise time curve which when plotted against time will give a Gaussian. Next this Gaussian curve is integrated and normalized. The results can be seen in Figure (13) where these points have been plotted against time on a probability paper. This procedure was repeated for the various voltages. These straight lines can give us information about the width of the Gaussian distribution as well as the centroid. As the voltage increases the slope of these lines increases. If we take the times that correspond to 50% level and we plot them against 1/v Figure (14) results. These points give the width (standard deviation) of the time distribution curves, or in other words the width indicates the time interval in which a pulse may cross the 50% level. When the voltage becomes larger this time gets shorter which shows that when the voltage becomes infinite the time should be very short, not zero of course, because we have to take into consideration the rise time of the amplifier.

Figure (15) shows total charge collection time against 1/v. These points were taken from Figure (12) as the time that the distribution reaches the highest point. From Figure

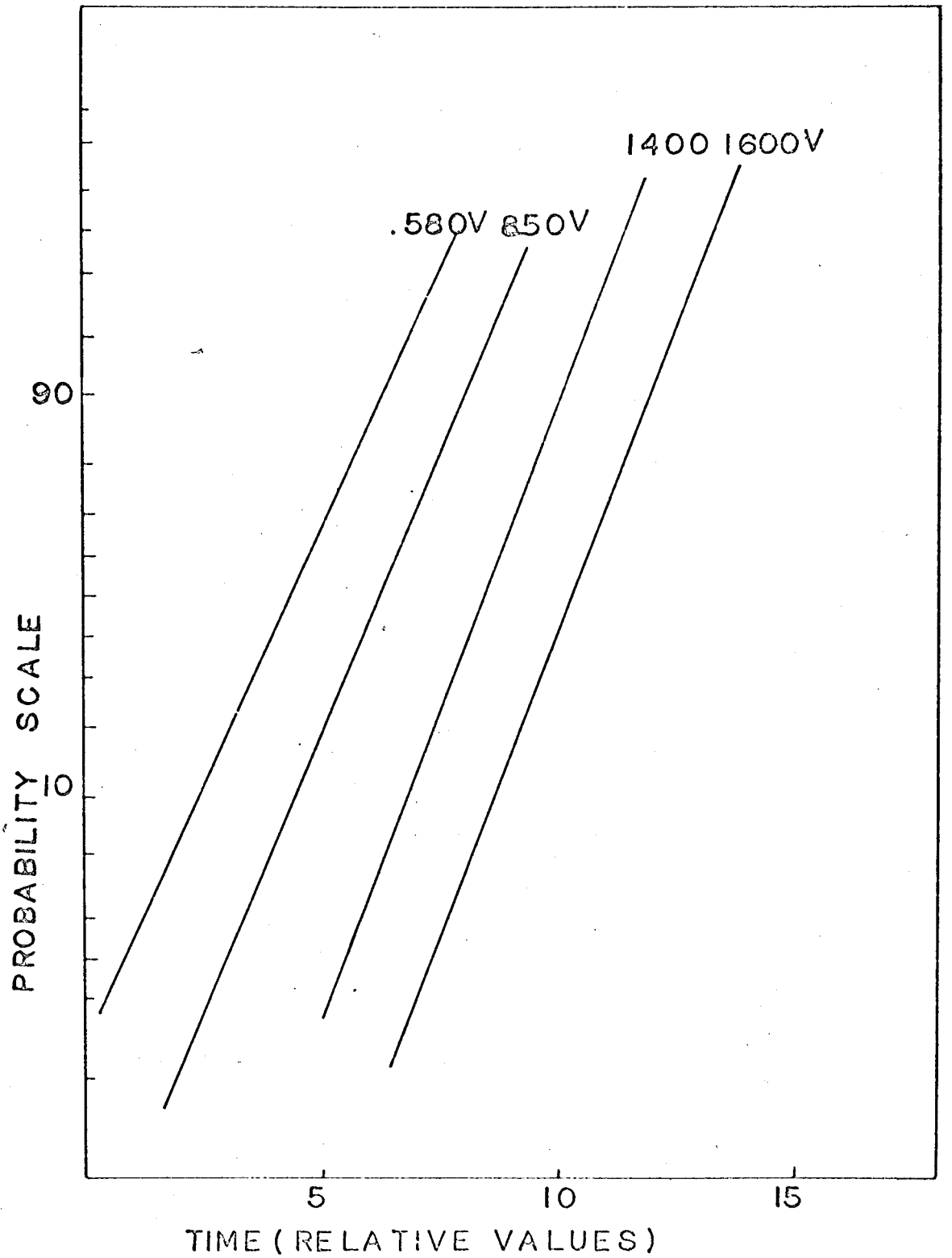

Fig. 13

Probability distribution

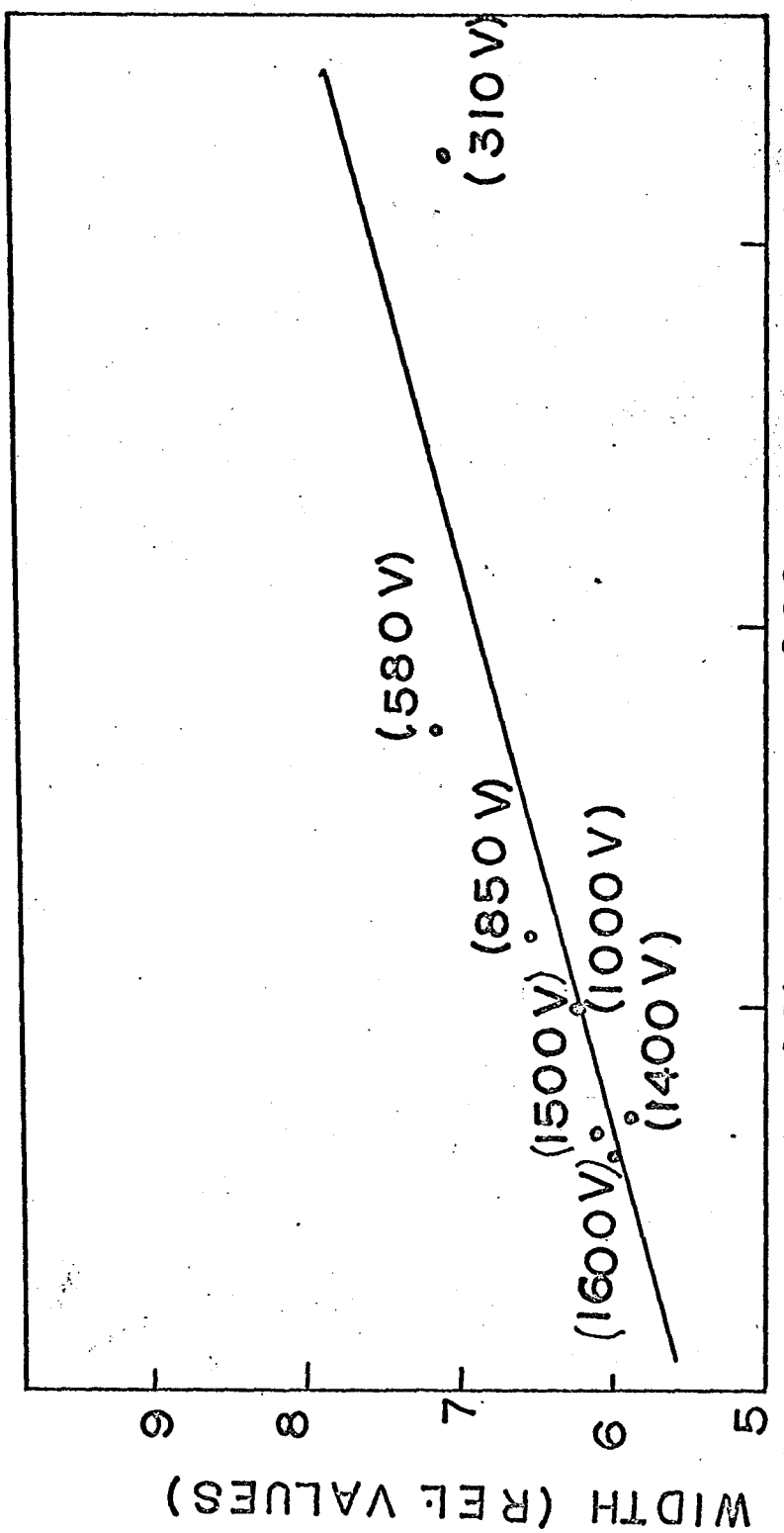

Fig. 14 Standard deviation against 1/V

(15) we come to the result that as the bias voltage increases the time gets shorter so the higher the voltage the less time it takes for the charge carriers to be collected by the electrodes. Thus,at low field intensities the detector seems to depart from the ideal response.

In Figure (11) four energy distribution curves have been plotted for various times. We are going to study now how the rise time variation produces variations in the pulse height distribution. So the centroid of every energy spectrum was calculated. These mean values were plotted against time. The results are shown in Figure (16) for various voltages. These distributions have been corrected by subtracting the background. We see that when the time increases the centroids get smaller; in other words the energy spectra are moving to the left, i.e.to apparently lower energy.

The breadth of the energy distribution curves about the mean value is expressed quantitatively by the standard deviation σ . A small σ gives a sharply peaked distribution, whereas a large σ gives a broad flattened distribution. So our next step is to calculate the standard deviations of the energy curves. The results are plotted against time (Figure (17)). It can be seen that the standard deviation increases with the time, therefore the energy spectra get broader as the time increases. This happens for all the seven various voltages. So we came to the result that the rise time

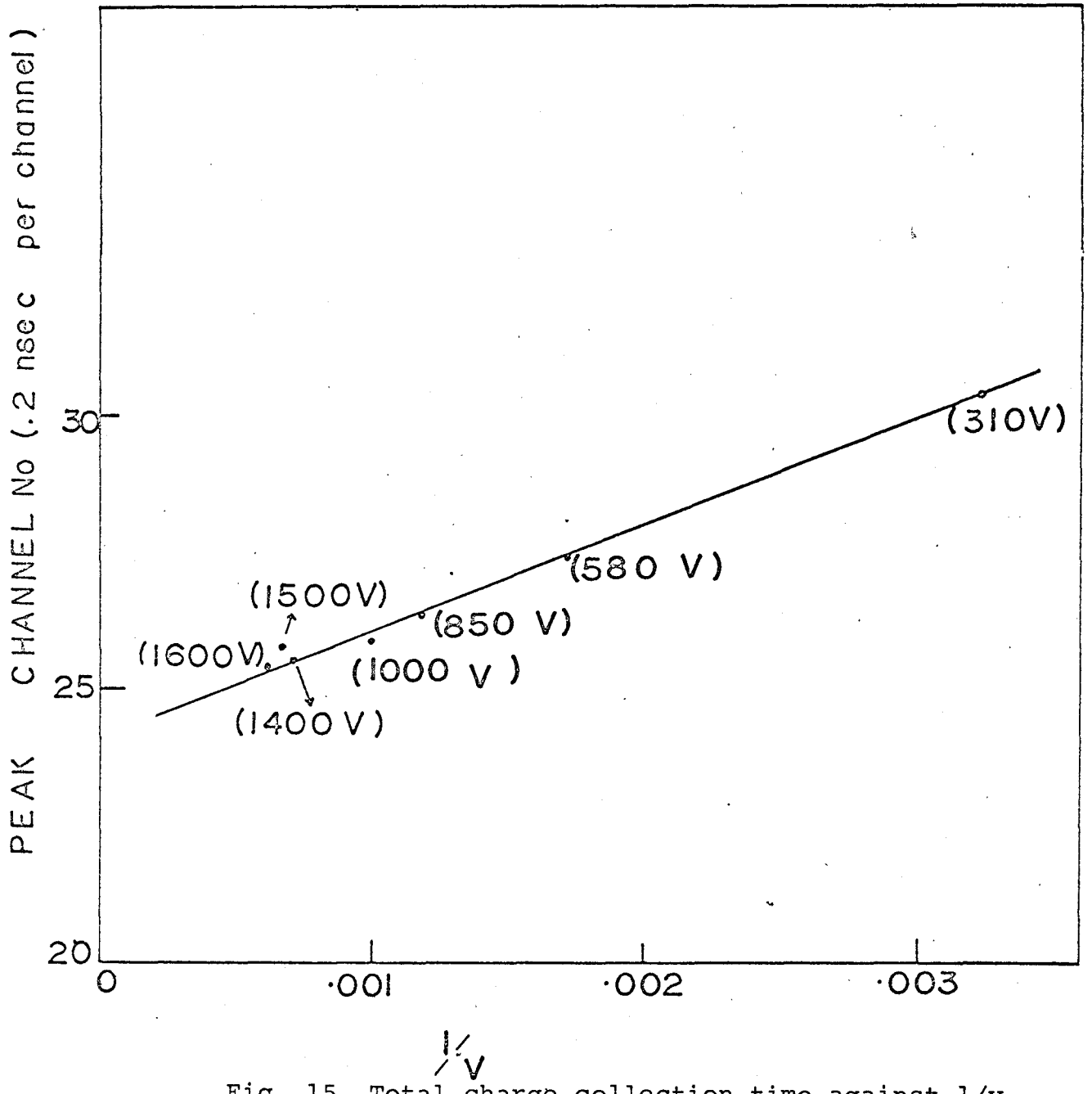

Fig. 15 Total charge collection time against 1/v

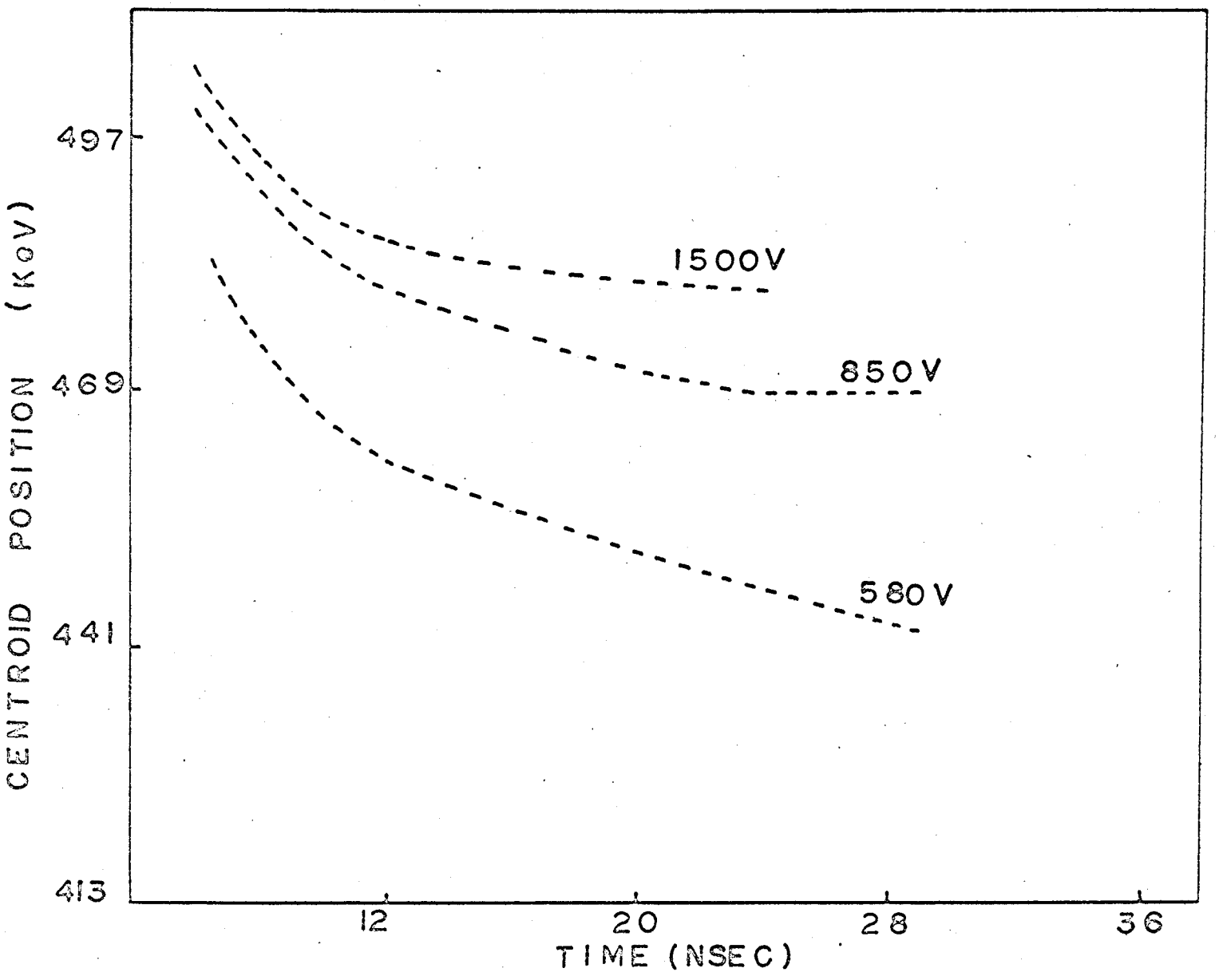

Fig. 16

Centroid of energy distributions against time for various voltages

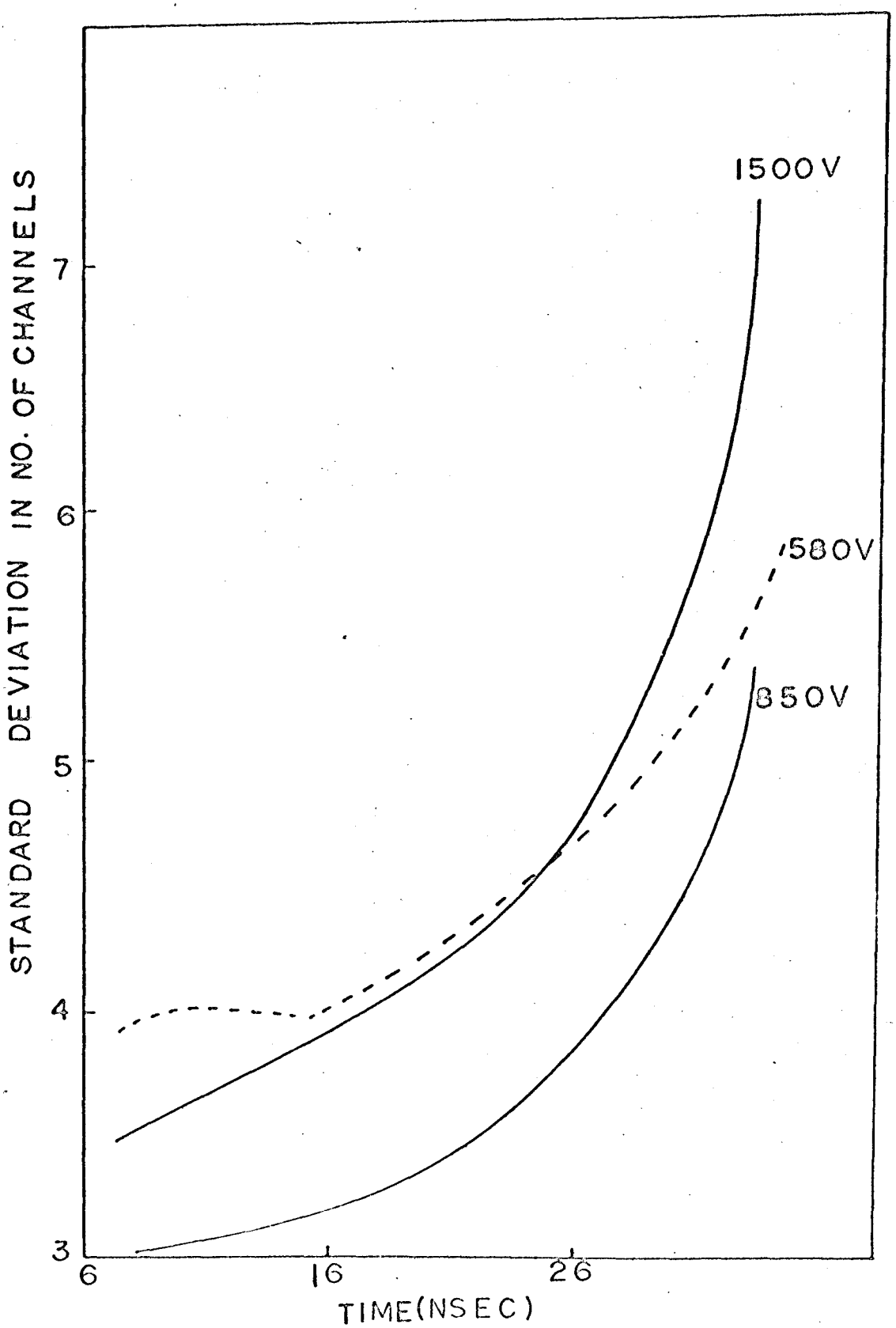

Fig. 17

Standard deviations of energy distributions against time for various voltages

variations produce consequential increase in the width of the pulse height distribution and therefore the energy resolution is affected.

4.3 Study of Ge(Li) Pulse Shapes

The previous investigations revealed that there is a positive correlation between energy and detection time. One can interpret this to indicate that slow rising pulses (which are created from interactions in low field regions) suffer more trapping and hence a net loss of charge carriers. While such a model will account for the observed results, a somewhat more rigorous demonstration was sought. Since our aim was to see if fast rising pulses yield more apparent energy than slower rising members the most obvious experiment was to examine pulse shapes and energy deposition.

An arrangement as illustrated in Figure (7) was used. While the sampling scope yields only one point on each coincidence pulse, the distribution of pulse shapes can be obtained. Two experiments were carried out in which pulses leading to energies in the photopeak were selected according to whether they were above or below the centroid. Real time experiments were conducted in which annihilation radiation was used through a ^{22}Na source.

The data obtained were normalized, and since events per unit time channel were constant, an integral represen-

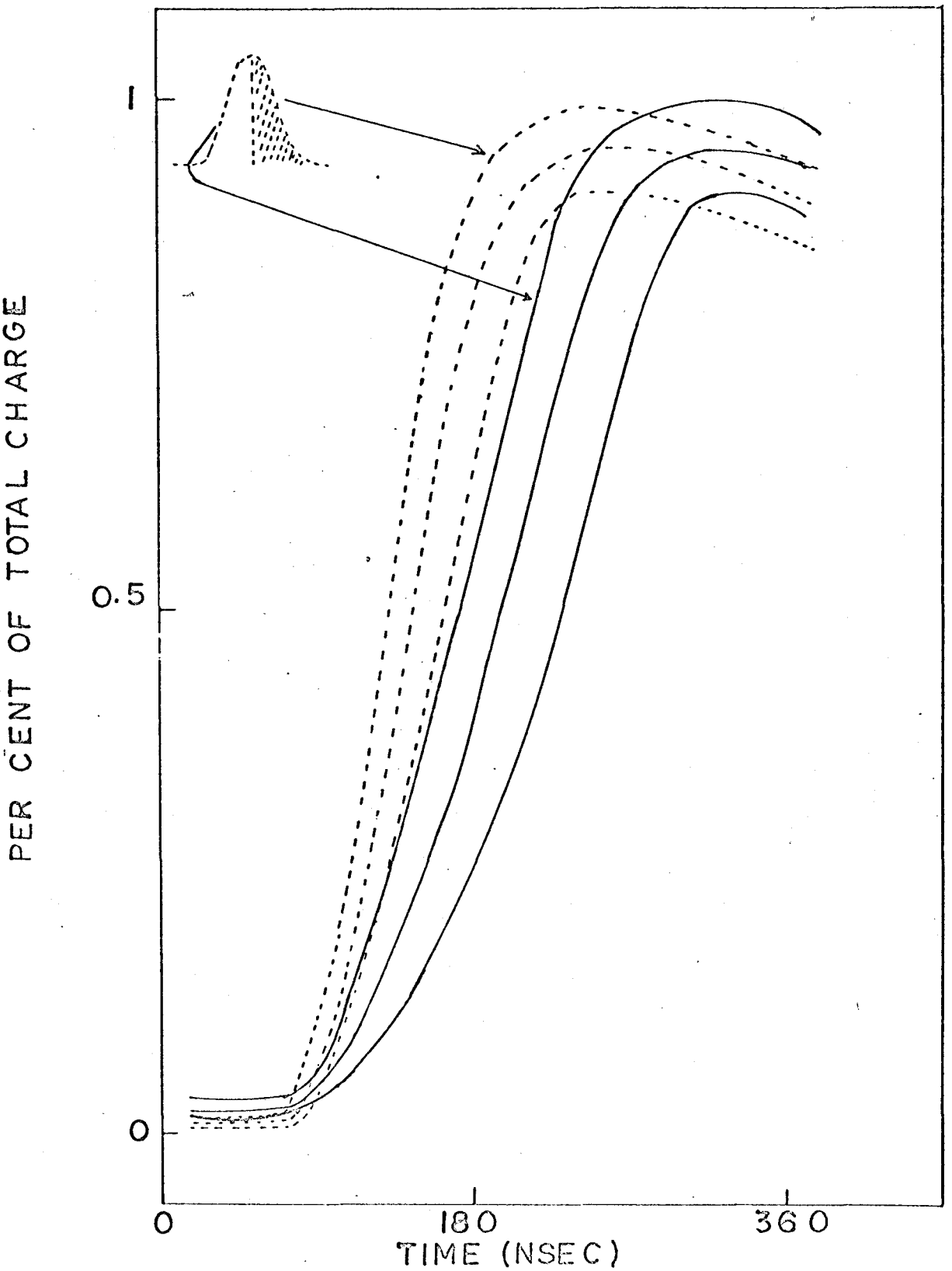

Fig. 18

Pulse shapes in ^{22}Na

tation calculated. Through interpolation "rise time profiles" for 20, 50 and 80 per cent of events were computed for both classes of energy, i.e. high and low side of photopeak. It is immediately apparent from Figure (18) that fast rising pulses are associated with above average energy deposition while for slow rising pulses the converse is true. Thus Figure (18) demonstrates the validity of the proposed explanation for the time-energy correlation observed across photo peaks.

If one examines the diffrerntial distribution of pulse rise times at constant fractional pulse height curves similar to those shown in Figure (18) are obtained. It is clear that low voltage triggering will lead to a minimum in timing uncertainty. The general shape of the pulses is similar to the calculated forms shown in Figure (18). The correlation of time and energy has resulted in a separation of pulses from events originating in regions near the junctions and regions of relatively uniform field distribution.

4.4 Results

From this study of the timing characteristics we came to the result that the single open-ended coaxial diodes with a trapezoidal cross section show some disadvantages for coincidence work. This is due to large variation in charge collection times which results from the non-uniformity of the

electric field. The non-uniformity of the electric field appears in the closed end of the detector. So we can have some improvement of the timing characteristics if we use longer coaxial diodes because, as it has been theoretically calculated in Chapter II, the spherical part is the one that gives the very slow pulses. Thus in a long coaxial diode the cylindrical part is extended. Also more improvement can be seen if we use coaxial diodes with two open ends because of the better uniformity of the electric field. Better timing characteristics have been found using double-open-end cylindrical detectors[10,11].

REFERENCES

(1) A.J. Tavendale and G. T. Ewan, Nuclear Instruments and Methods 25 (1963) 185.

(2) A. J. Tavendale, IEEE Transactions on Nuclear Science, NS-11, No. 3 (1964) 191.

(3) A. J. Tavendale, IEEE Transactions on Nuclear Science, NS-12, No. 1 (1965) 255.

(4) H. L. Malm, A.J. Tavendale and I. L. Fowler, Canadian J. Phys. 43, 1173 (1965).

(5) A. J. Tavendale, IEEE Transactions on Nuclear Science, NS-13, No. 3 (1966) 315.

(6) G. Armantrout, IEEE Transactions on Nuclear Science, NS-13 (1966) 84.

(7) H. J. Fiedler, L. B. Hughes, T.J. Kennett, W. V. Prestwich and B. J. Wall, Nuclear Instruments and Methods 40, No. 2 (1966).

(8) M. G. Strauss, R. N. Larsen and L. L. Sifter, IEEE Transactions on Nuclear Science, NS-13, No. 3 (1966) 265.

(9) E. Sakai and T. A. McMath, Nuclear Instruments and Methods, 64 (1968) 132.

(10) H. L. Malm, IEEE Transactions on Nuclear Science, NS-13, No. 3 (1966) 285.

(11) G. T.Ewan, R. L. Graham and I. K. Mackenzie, IEEE Transactions on Nuclear Science, NS-13, No. 3 (1966) 297.

(12) E. Sakai, IEEE Transactions on Nuclear Science, NS-15, No. 3 (1968) 310.

(13) P. P. Webb, H. L. Malm, M. G. Chartrand, R. M. Green, E. Sakai and I. L. Fowler, Nuclear Instruments and Methods, 63 (1968) 125.

(14) J. Pigneret, J.J. Samuel and A. Sarazin, IEEE Transactions on Nuclear Science, NS-13, No. 3 (1966) 306.

(15) F. S. Goulding, Lawrence Radiation Laboratory Report UCRL-16231 (1965).

(16) H. Delyser, F. P. Ziemba and W. R. Van Antwerp, IEEE Transactions on Nuclear Science, NS-12, No. 1 (1965) 265.

(17) T.J. Kennett, W. V. Prestwich, Nucleonics 23, No. 5 (1965) 265.

(18) D. N. Poenaru, IEEE Transactions on Nuclear Science, NS-14, No. 5 (1965) 1.

(19) M. G. Strauss, Rev. Sci. Instr. 34, 1248 (1963).

(20) G. Dearnaley and D. C. Northrop, Semiconductor Counters for Nuclear Radiations, Spon Press, London (1964).

(21) R. L. Graham, I. K. Mackenzie, and G. T. Ewan, IEEE Transactions on Nuclear Science, NS-13, No. 1 (1966) 72.

(22) M. G. Strauss and R. N. Larsen, Nuclear Instruments and Methods 56 (1967) 80.

(23) R. L. Chase, Nuclear Pulse Spectrometry. McGraw-Hill,(1961).

(24) A. B. Gillespie, Signal, Noise and Resolution in Nuclear Counter Amplifiers. McGraw-Hill, (1953).